16. SUCCESSIVE SPHERE SOLUTIONS

The final step in the main astrometric reductions was the combination of the reference great-circle data sets accumulated throughout the mission into a coherent set of astrometric parameters for stars on the whole sky. The principles of this 'sphere solution' process were described in Chapter 11. In the course of the Hipparcos mission several successive sphere solutions were made independently by the FAST and NDAC consortia, involving successively larger data sets or iterations of the main reduction chain. The completion of the solutions using 12, 18, 30 and (finally) 37 months of data provided important checkpoints for the validation of the reductions, and allowed the progress of the astrometric analysis to be followed in terms of the improving statistics of the FAST/NDAC differences. In this chapter the main features of the successive sphere solutions are summarised, results of the main comparisons are presented, and the various sphere solutions are compared with the final Hipparcos Catalogue.

16.1. Introduction

The series of sphere solutions described and compared in this chapter resulted from the incorporation of successively more observations, from iterations of the previous steps of the reduction chain (attitude determination and great-circle reductions), and from improvements of the weighting schemes and modelling of instrumental effects. The evolution of the astrometric data in these solutions, and particularly of the FAST/NDAC differences, strikingly illustrates the convergence of the two complex and rather different reduction schemes into a single, final catalogue.

The principles of the sphere solution are summarised in Chapter 11. The term is used here in a broad sense, including both the determination of the abscissa zero points of the reference great circles (the sphere solution proper) and the subsequent determination of astrometric parameters for individual stars. In the FAST reduction chain these two processes were seen as separate tasks, while in NDAC they were combined in a single task. In both cases the end result was a set of astrometric parameters, in which all the positions and proper motions were given in one and the same reference frame—albeit that frame was not the same in FAST and NDAC, and indeed changed slightly for each new sphere solution. The indefiniteness of the reference frame is inherent to the principle of Hipparcos observations, where a star was only measured relative to other stars and never linked directly to any point with *a priori* known position or proper motion. Ideally, however, the reference frames of any two sphere solutions should differ

only by a rigid-body rotation, which is expressed by six numbers (Section 16.6). After elimination of this rotation difference, the differences in position and proper motion may be analysed in terms of random, regional and global differences. In this chapter the successive sphere solutions obtained by FAST and NDAC have all been aligned with the final Hipparcos Catalogue prior to the comparisons (see Table 16.8).

In contrast with the positions and proper motions, where no 'origin' is accessible to observation by Hipparcos, the trigonometric parallaxes obtained in the reductions are in principle absolute. The comparison of parallaxes is therefore quite straightforward.

Major milestones of the astrometric reductions were reached with the completion of the FAST and NDAC sphere solutions using 12, 18, 30 and (finally) 37 months of data. The main features of these solutions are described in Sections 16.3 to 16.5 and the main results of their intercomparison are given in Section 16.6. For completeness the final Hipparcos Catalogue (HIP) and the two preliminary merged catalogues H18 and H30 are included in the comparisons.

16.2. Principles of Iterations

The astrometric reductions for the Hipparcos mission were global in the sense that the astrometric parameters—positions, parallaxes and proper motions—of a large number of stars scattered over the whole celestial sphere had to be solved together. This was necessary in order to achieve a globally consistent system of positions and proper motions, and for the determination of absolute parallaxes. It was not necessary, though, that this solution included all the objects observed with the satellite: special objects like double and multiple stars, stars showing non-linear photocentric motions, and solar system objects could be linked into the same system at later stages of the reductions. In principle this global solution should have used all the data collected throughout the mission in order to obtain the optimum estimate of each parameter. The number of essentially 'non-problematic' stars suitable for this process was about 100 000. Thus, a rigorous implementation of such a solution would have involved the simultaneous adjustment of some 500 000 stellar parameters plus many more describing the instrument and its scanning motion, using the observation frames as input for the adjustment.

At the time when the software for the Hipparcos data reductions was designed, the rigorous adjustment of such a large problem was not considered feasible. An alternative, less rigorous but practicable method was devised, usually referred to as the 'three-step' reduction procedure (Section 4.1). The main idea was to introduce an intermediate level of adjustment, where instantaneous, one-dimensional stellar coordinates along selected reference great circles were estimated; these coordinates are known as the star abscissae. The need to iterate the main astrometric reductions was a direct consequence of this simplified approach adopted by both the FAST and NDAC consortia. Its principle can be understood as follows.

The elementary Hipparcos observations were one-dimensional, measuring the location of stars in the direction G perpendicular to the slits of the main grid (Figure 16.1). In the great-circle reduction, these measurements were combined into estimates of the star abscissae along the reference great circle. However, because the slits generally made a small angle φ relative to the lines of constant abscissae, the observed quantity G depended not only on the abscissa v but also, to a smaller extent, on the distance of

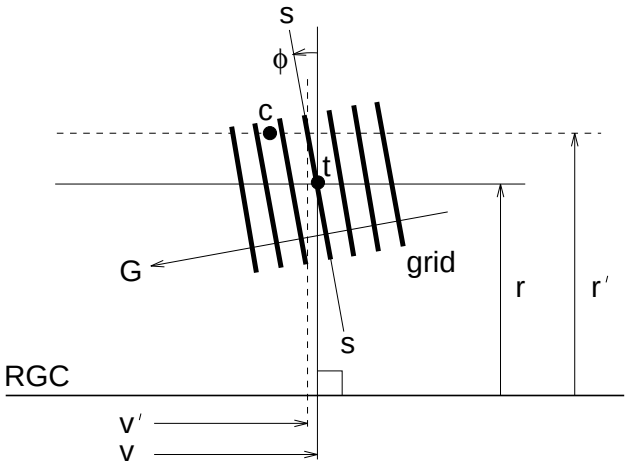

Figure 16.1. *Schematic illustration of the abscissa projection error in the great-circle reduction caused by catalogue errors. RGC = reference great circle; t = true position of star; c = star position according to the current catalogue;* (v, r) *= true abscissa and ordinate of the star;* r' *= assumed ordinate (computed from the catalogue); ss = observed location of the star (from measurement of the G coordinate);* v' *= inferred abscissa. The error in the inferred abscissa is given by* $v' - v = -(r' - r)\sin\varphi$.

the star from the reference great circle, i.e. on the ordinate r. Since r was not estimated in the great-circle reduction, it had to be computed from the current knowledge of star positions and instrument attitude. As illustrated in Figure 16.1 the error in the ordinate, $r' - r$, was transferred into an error in the estimated abscissa through a multiplicative factor of about $\sin\varphi$. (More accurately, the effective factor was a mean value $\langle\sin\varphi\rangle$ over all the scans across the star considered in the great-circle reduction. This averaging greatly reduced the resulting error for many stars.)

The reference great circles were generally chosen such that $|\varphi| \lesssim 1°$. Consequently the catalogue-induced abscissa errors were at most some 2 per cent of the positional errors of the catalogue used in the great-circle reduction. The rms contribution to the abscissa errors was typically about 0.7 per cent of the catalogue errors (van der Marel 1988). Similar considerations can be made for the attitude errors, where the error component normal to the scanning was propagated into the abscissae with a corresponding attenuation factor. In the subsequent sphere solution the standard errors of the astrometric parameters were normally a factor $\simeq 0.2$ smaller than the standard errors in abscissae. Thus, the total attenuation factor for the positional errors, when propagated from an initial catalogue through the attitude determination, great-circle reductions and sphere solution, was typically of the order of 0.1 to 0.2 per cent. This is to be regarded as a gross average; on specific stars the situation may have been much less favourable.

Initially, the astrometric data in the Hipparcos Input Catalogue were used to determine the satellite attitude and in the preliminary great-circle reductions. The positional uncertainty of that catalogue, at the epoch 1990.0, was typically about 0.3 arcsec (Turon *et al.* 1995), with zonal systematic errors reaching 0.2 arcsec and with individual errors up to several arcsec. The corresponding errors after a first sphere solution should therefore generally be of the order of 0.5 mas, but perhaps reaching several milliarcsec on some stars. This is not negligible compared with the level of errors expected from the photon noise, instrument modelling, etc., and the obvious remedy was iteration: the

Table 16.1. Summary of successive NDAC and FAST sphere solutions, and of the three merged catalogues H18, H30 and HIP. The initial letter in the solution designations indicates the origin: NDAC (N), FAST (F), or merged (H). The following number is the approximate number of months of observations that were used in the solution, with a decimal indicating an iterated or otherwise improved version. 'R' signifies restricted solutions, solving only for positions and parallaxes (with proper motions taken from the Hipparcos Input Catalogue). N0R is the solution based on the validation data. Subsequent columns give the approximate date of the solution; the number of stars with accepted astrometric solutions; the total number of abscissae input to the sphere solution, and the number of abscissae actually used for the accepted stars; the range and number of orbits used; and the reference epoch for the resulting astrometric parameters. Concerning the range of orbit numbers it can be noted that no data exist from orbits 2 to 47. The Julian Date for the apogee of orbit number N is approximately given by $2\,447\,835.46 + 0.4441N - 1.3 \times 10^{-7} N^2$.

Solution	Approx. date of creation	No. of stars	No. of absc. (input)	No. of absc. (used)	Range of orbits	No. of orbits	Ref. epoch
N0R	27 May 1991	15 564	269 769	81 704	1–1032	171	1990.00
N12	28 Apr 1992	47 061	1 312 713	667 447	1–915	812	1990.00
N12R	12 May 1992	82 309	1 312 713	996 511	1–915	812	1990.00
N18	14 Oct 1992	102 411	1 979 988	1 792 839	1–1336	1215	1990.00
N30	22 Sep 1993	103 131	3 158 933	2 876 215	1–2118	1963	1990.00
N37.1	30 Sep 1994	109 698	3 632 162	3 463 106	1–2768	2328	1990.00
N37.5	25 Apr 1995	111 255	3 570 685	3 490 792	1–2768	2326	1991.25
F12	30 Apr 1992	31 921	1 226 986	424 227	48–925	758	1992.00
F12R	1 Jul 1992	46 716	1 226 986	505 885	48–925	758	1992.00
F18	25 Oct 1992	93 781	1 952 958	1 597 519	48–1336	1184	1990.75
F18.1	23 Jun 1993	93 612	1 952 958	1 573 013	48–1336	1177	1990.75
F30	27 Sep 1993	99 950	3 221 747	2 670 741	48–2129	1914	1991.25
F37.1	22 Oct 1994	117 246	3 724 992	3 592 389	48–2763	2269	1991.25
F37.3	13 Jun 1995	116 683	3 743 053	3 570 708	48–2763	2281	1991.25
H18	23 Sep 1993	105 371			1–1336		1990.75
H30	11 Jan 1994	107 504			1–2129		1991.25
HIP	8 Jun 1996	117 955			1–2768		1991.25

star positions resulting from the first sphere solution were used for an improved attitude determination, improved great-circle reductions, and an improved sphere solution. In principle a single such iteration might be sufficient to ensure that the resulting sphere solution is completely limited by observational noise, and independent of the starting values used for the astrometric parameters. However, as is generally the case in complex iterations, some error components decay much slower than the overall variance, and at least two complete iterations were considered necessary in the case of the Hipparcos reductions. In reality these iterations were important also for many other aspects of the reductions, in particular the instrument calibrations, which depended critically on the accuracy of the star catalogue being used.

The sphere solutions discussed in this chapter are summarised in Table 16.1 and further described in subsequent sections. Some entries in the Hipparcos Catalogue are clearly unsuitable for comparison with the earlier sphere solutions, because they finally required more complex modelling than the standard five-parameter astrometric model assumed in the sphere solution. This applies in particular to well-resolved double stars, orbital binaries, variability-induced movers (VIMs), and stochastic solutions (see Volume 1, Section 2.3 for an explanation of these categories). The statistics and comparisons given below are therefore restricted to the basic subset of 101 246 entries whose data

were, in the final catalogue, adopted from the astrometric merging process using the five-parameter model. The basic subset was extracted from the 117 955 entries in the Hipparcos Catalogue with astrometric data, by requiring that either Field H59 is blank (meaning that the entry is not part of the Double and Multiple Systems Annex), or that Field H60 = 'S' (meaning that the star was resolved as a close binary, but that its photocentre was solved with the standard five-parameter model). Statistics referring to the whole Hipparcos Catalogue are found in Volume 1, Part 3.

16.3. NDAC Sphere Solutions

Overview of Iterations

The NDAC iteration scheme deviated somewhat from the principle described in the previous section. In parallel with the star mapper data processing and attitude determination performed at the Royal Greenwich Observatory, a working star catalogue was maintained and successively updated by means of the star mapper transit residuals obtained in the attitude fit (Section 6.9; see also van Leeuwen *et al.* 1992). During the first 18 months of the mission this catalogue provided far better positions than the Input Catalogue for many stars, and these were used in the NDAC great-circle reductions until superseded by the first full-scale sphere solution (N18). Compared with the FAST scheme this gave a rapid initial improvement of the data, but relatively smaller improvements by the later sphere solutions.

Subsequent processing in NDAC was based on the N18 catalogue (actually on a slightly later version including about six weeks of additional data), including a re-run of the great-circle reductions for the first part of the mission. This resulted first in the 30-months solution N30, and, after all the mission data had been been included (approximately 37 months in all), the solution N37.1. That catalogue was then used for a third and final re-run of the attitude determination and great-circle reductions. The resulting abscissae were used in a series of sphere solutions leading up to the final NDAC solution N37.5. Versions N37.2 to N37.5 used the same abscissa data as input and differed mainly in the treatment of colour terms and in the internal weighting of data, as outlined below.

Main Characteristics of the Solutions

N0R: This was the partial sphere solution based on the so-called validation data given to the reduction consortia prior to the full-scale data distribution. The purpose of the validation data was to test the interfaces between ESOC and the reduction consortia, to enable the consortia to test their software for the first time on 'real' data, and to make cross-comparisons of the intermediate results in order to validate the satellite data. The analysis of the validation data was in NDAC carried all the way through the main reduction chain, up to the sphere solution, in spite of the very scant sky coverage. This provided a very important first check of the overall consistency of the data, as discussed by Lindegren *et al.* (1992).

N12 and N12R: Both these solutions were based on the same set of abscissae from about 12 months of data collected up to 16 December 1990. In N12 all five astrometric parameters were solved whenever possible; in N12R the proper motions were constrained to

their values in the Input Catalogue and only the positions and parallaxes were updated, which allowed many more stars to be treated. The criteria for accepting the astrometric solution on a specific star included an upper limit on the standard error in parallax, $\sigma_\pi \leq 4$ mas in N12 and $\sigma_\pi \leq 3$ mas in N12R, and on the goodness-of-fit statistic, F2 ≤ 5 (for a definition of F2, see the description of Field H30 in Volume 1). Some stars were also rejected because of unreasonably large updates in position or proper motion.

Previous sphere solutions had shown that the abscissa variances estimated in the great-circle reductions (for the 'smoothed' solutions) were systematically too small, and that an extra variance of $(2.7 \text{ mas})^2$ had to be added to obtain a reasonable agreement with the distribution of residuals. This weight correction was used in N12 and subsequent NDAC sphere solutions, until an improved weighting scheme was introduced with N37.1 (see below).

N18: This solution was based on about 18 months of data, including observations made up to 21 June 1991. All five astrometric parameters were estimated. The acceptance criteria included limits on the standard errors in parallax ($\sigma_\pi \leq 4$ mas) and proper motion ($\sigma_{\mu_{\alpha*}}$, $\sigma_{\mu_\delta} \leq 15$ mas/yr), and on the correlations between parallax and proper motion ($|\rho_\pi^{\mu_{\alpha*}}|$, $|\rho_\pi^{\mu_\delta}| \leq 0.6$).

N30: Observations collected up to 2 June 1992 were included in this sphere solution, which was the first complete NDAC iteration in the sense that the attitude determination and great-circle reductions had been re-computed with a star catalogue based on a full-scale sphere solution ($\simeq$ N18).

N37.1: The NDAC 37-months solutions include data collected up to the actual end of the scientific operations on 17 March 1993. Starting with N37.1, several improvements were made in order to obtain valid solutions for as many stars as possible, and to further reduce modelling errors. The improvements included in particular: relabelling and merging of data for some stars which for historical reasons had been observed under two different identifiers; resolution of grid-step errors remaining from previous solutions; inclusion of the sixth harmonic terms estimated for individual reference great circles; introduction of non-zero assumed radial velocity for 22 stars (see Volume 1, Table 1.2.3); and the use of $V-I$ colours (instead of B_T-V_T) as the basis for chromaticity calibrations. The previous upper limits on acceptable astrometric standard errors and correlations were also removed and replaced by a flagging of weak solutions.

N37.5: The solution N37.1 was used for a complete iteration of the attitude determination and great-circle reductions. The resulting abscissae were used as input for N37.2 to N37.5, a series of sphere solutions in which the final treatment of chromatic effects, the sixth harmonic, and the weighting of the abscissae were fixed after considerable experimentation. Starting with N37.2, the adjustment of the astrometric parameters were directly made with respect to the epoch J1991.25(TT), thus eliminating the need for epoch transformations on the resulting catalogue. Each solution produced summary statistics of the $\simeq$ 3.5 million abscissa residuals binned according to colour ($V-I$), magnitude (Hp), and orbit number; they were also analysed by linear regression versus $\cos 6\nu$ and $\sin 6\nu$ for each great-circle reduction. The trends in terms of biases and deviations from the expected unit weight residual were carefully studied and, when relevant, incorporated as systematic corrections to the abscissae and their standard errors in a subsequent solution. What was finally obtained (in N37.5) was therefore an internally consistent solution with an overall unit weight error of 1.000 and with no significant

trends with magnitude and colour. The re-calibration of abscissa standard errors between N37.1 and N37.5 resulted in a general decrease by about 14 per cent of the formal standard errors of the astrometric parameters, although the actual improvement of the astrometric parameters was probably very marginal (see Section 16.5).

The solution N37.5 also produced output, in the form of adjusted parameters and residuals, that was used for the final merging of the FAST and NDAC astrometry (Chapter 17) and for the production of the Hipparcos Intermediate Astrometric Data (Volume 1, Section 2.8).

Treatment of Chromaticity

Both N12 and N12R included, as the only global parameters, the unknowns Γ_{23} and Γ_{24} which model an abscissa bias varying linearly with colour index and time:

$$v^{\rm obs} = v^{\rm calc} + \Gamma_{23} C + \Gamma_{24}(t - 1990.5)C + \eta \qquad [16.1]$$

Here $v^{\rm obs}$ is the observed abscissa, $v^{\rm calc}$ the abscissa calculated from all parameters except the global ones, $C = (B_T - V_T) - 0.5$, t is the time of the observation, and η is the abscissa noise. Colour indices $B_T - V_T$ were generally taken from the Extended Input Catalogue (Perryman *et al.* 1989 Volume II, Section 18.2), with some updates resulting from the star mapper photometric processing. The results for the chromaticity were rather similar in the two solutions:

$$\left.\begin{aligned} \Gamma_{23} &= -1.355 \pm 0.015 \text{ mas mag}^{-1} \\ \Gamma_{24} &= +0.339 \pm 0.100 \text{ mas mag}^{-1} \text{ yr}^{-1} \end{aligned}\right\} \quad \text{N12} \qquad [16.2]$$

$$\left.\begin{aligned} \Gamma_{23} &= -1.425 \pm 0.009 \text{ mas mag}^{-1} \\ \Gamma_{24} &= +0.313 \pm 0.038 \text{ mas mag}^{-1} \text{ yr}^{-1} \end{aligned}\right\} \quad \text{N12R} \qquad [16.3]$$

Solution N18 contained the same chromatic terms (along with additional parameters discussed below), and the result agrees well with the earlier determinations:

$$\left.\begin{aligned} \Gamma_{23} &= -1.404 \pm 0.007 \text{ mas mag}^{-1} \\ \Gamma_{24} &= +0.330 \pm 0.020 \text{ mas mag}^{-1} \text{ yr}^{-1} \end{aligned}\right\} \quad \text{N18} \qquad [16.4]$$

From N30 onwards, the reference epoch for Γ_{23} was taken to be J1991.25 instead of J1990.5. The result for N30 was:

$$\left.\begin{aligned} \Gamma_{23} &= -1.110 \pm 0.004 \text{ mas mag}^{-1} \\ \Gamma_{24} &= +0.366 \pm 0.007 \text{ mas mag}^{-1} \text{ yr}^{-1} \end{aligned}\right\} \quad \text{N30} \qquad [16.5]$$

corresponding to the value -1.385 ± 0.007 mas/mag at J1990.5. In N37.1 the colour index $V - I$ was used instead of $B_T - V_T$, resulting in a slight change in the numerical values:

$$\left.\begin{aligned} \Gamma_{23} &= -1.166 \pm 0.006 \text{ mas mag}^{-1} \\ \Gamma_{24} &= +0.332 \pm 0.007 \text{ mas mag}^{-1} \text{ yr}^{-1} \end{aligned}\right\} \quad \text{N37.1} \qquad [16.6]$$

Using the same abscissa input as for the 30-month solution, a special solution was made in order to investigate the dependence of the chromatic displacement on the colour index. In this solution a sixth parameter (a_6) was added for each star, while no global chromatic terms were used. With $v^{\rm calc}$ denoting the abscissa calculated without any chromatic term, using the normal five astrometric parameters (a_1 to a_5), the observation equation for the additional parameter was written:

$$v^{\rm obs} = v^{\rm calc} + [-1.110 + 0.366(t - 1991.25)]a_6 \qquad [16.7]$$

According to Equation 16.5 the coefficient in brackets equals the mean chromatic displacement per magnitude in $B_T - V_T$, assuming that the effect depends linearly on that colour index. The standard errors of the individual estimates of a_6 were typically around 0.8 mas, or 0.8 mag if the parameter is interpreted as a colour index. Mean relations between a_6 and the colour indices $B_T - V_T$ and $V - I$ are shown in Figures 16.2–16.3. It appears that the relation to $V - I$ is the more linear one, at least for the very red stars, which motivated the switch from $B_T - V_T$ to $V - I$ from N37.1. However, both relations show some significant curvature and kinks in the well-determined colour interval.

It was suggested by M. Grenon that the effective wavelength might be a better independent variable for modelling the chromatic abscissa displacement, and formulae for calculating $\lambda_{\rm eff}$ as function of $V - I$ and t were provided. A simple transformation of the $V - I$ scale in Figure 16.3 into the effective wavelength at mid-mission indicated that $\lambda_{\rm eff}$ probably gives the best overall linear representation of the effect (Figure 16.4). In N37.5 the independent variable for the chromatic displacement was taken to be the dimensionless quantity $[\lambda_{\rm eff}(V - I, t) - 550\ {\rm nm}]/(50\ {\rm nm})$, replacing the $(V - I) - 0.5$ used in N37.1.

Preliminary runs with all 37 months of data indicated that the chromatic behaviour of the instrument changed towards the end of the mission, and that a simple linear variation of the chromaticity with time would no longer be sufficient. Figure 16.5 shows the chromaticity obtained for the individual great-circle reductions by regression of the abscissa residuals against $\lambda_{\rm eff}$. The roughly linear variation up to day 1170 (mid-March 1992) agrees well with the previously determined Γ_{23} and Γ_{24}, but this trend is then replaced by a rather erratic behaviour. Much of the scatter seen in this figure is actually physically significant and anomalous variations can be discerned also earlier in the mission, especially around day 490 (April–May 1990). The chromatic modelling was therefore modified to include an *a priori* correction for the individual orbits, on top of which the global parameters Γ_{23} and Γ_{24} were determined. The relevant terms in the observation equations were therefore written:

$$v^{\rm obs} = v^{\rm calc} + \left[Q_N + \Gamma_{23} + \Gamma_{24}(t - 1991.25)\right] \frac{\lambda_{\rm eff} - 550\ {\rm nm}}{50\ {\rm nm}} + \eta \qquad [16.8]$$

where Q_N is the *a priori* chromaticity in orbit N shown in Figure 16.5. The chromatic parameters were found to be:

$$\left.\begin{array}{l} \Gamma_{23} = +0.049 \pm 0.004\ {\rm mas} \\ \Gamma_{24} = +0.010 \pm 0.005\ {\rm mas\ yr^{-1}} \end{array}\right\} \quad {\rm N37.5} \qquad [16.9]$$

In principle these parameters should vanish in view of the *a priori* correction of chromaticity through Q_N. The above values, being below the 0.1 mas level, were however considered acceptable.

Harmonic Terms

The harmonic terms are systematic displacements of the abscissae which are periodic functions of the abscissa difference between the star and the Sun, $v - v_\odot$. Consideration of possible thermally induced variations of the basic angle, related to the satellite/Sun geometry, led to the introduction of the global parameters Γ_2 to Γ_{12}, which express such a variation up to the sixth harmonic, assuming phase coherence over the whole mission (Lindegren *et al.* 1992). These parameters were included in solution N0R and N18. In N18 all eleven parameters were smaller than 0.1 mas in absolute value, although some

of them were formally significant. Special tests were also carried out: the 18 months of data were split into odd- and even-numbered reference great circles, and independent sphere solutions were calculated for the two data sets. The global harmonic parameters were found to be rather different in the two solutions, supporting the conclusion that none of them were really significant. In subsequent solutions no global harmonic term was therefore included.

While systematic variations related to the satellite/Sun geometry thus appeared to be negligible, the abscissa residuals for individual great-circle reductions often showed a pronounced pattern with a dominant period of 60° (the 'sixth harmonic'). This can be understood as an effect of the relative difficulty in estimating this particular harmonic component of the abscissae, which in turn is related to the particular value of the basic angle, $\simeq 58°$. In different great-circle reductions the sine and cosine components of the sixth harmonic are excited by unpredictable causes and therefore result in a quasi-random distribution of phases. This explains why the global parameters Γ_{11} and Γ_{12} were small, even if the effect was large on individual great circles. The amplitude of the sixth harmonic was typically about 2 mas, but may reach 10 to 20 mas in some great-circle reductions. In the 37-month solutions the coefficients of the sixth harmonic were determined independently for each great-circle reduction by analysis of the residuals. The corresponding harmonics were then removed in the subsequent solution. This process had essentially converged before the calculation of the final solution N37.5.

Gravitational Deflection

Solutions N30, N37.1 and N37.5 included the global parameter Γ_{13}, which is a correction to the general-relativistic light deflection (Perryman *et al.* 1989 Volume III, Section 9.3). It is related to the PPN parameter γ by:

$$\gamma = 1 + \frac{Ac^2}{2GS}\Gamma_{13} \qquad [16.10]$$

where $2GS/Ac^2 = 4.0719\ldots$ mas is the deflection at right angles to the solar direction for an observer at one astronomical unit (A) from the Sun (see also Equation 11.19). The following values were obtained:

$$\begin{aligned} \gamma &= 0.971 \pm 0.006 \quad (\text{N30}) \\ \gamma &= 0.993 \pm 0.007 \quad (\text{N37.1}) \\ \gamma &= 0.992 \pm 0.005 \quad (\text{N37.5}) \end{aligned} \qquad [16.11]$$

The reason for the rather low value of γ in N30 is not known; possibly it is related to the modelling of the sixth harmonic, which was introduced with N37.1. The other two values are not significantly different from unity, as predicted by General Relativity.

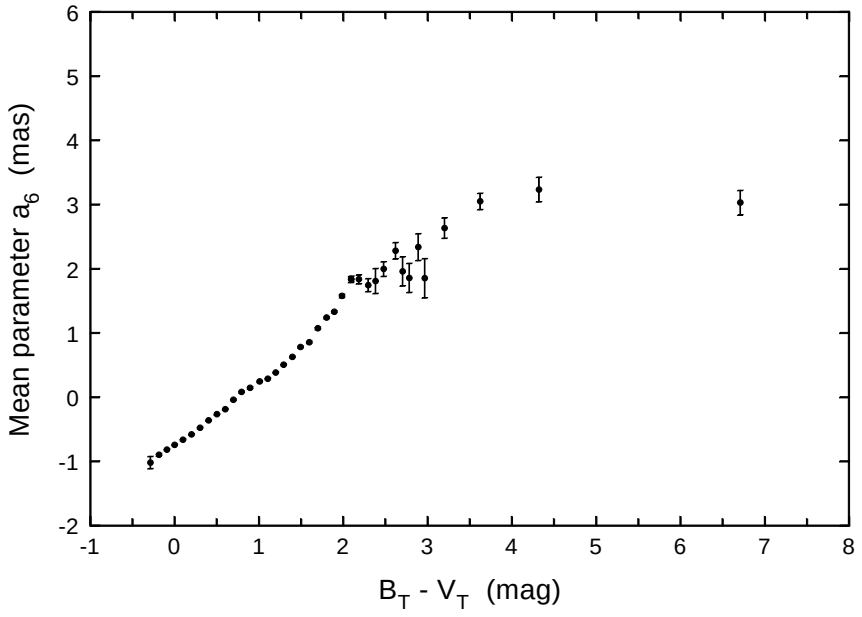

Figure 16.2. *The chromatic effect studied by solving the abscissa displacement for each star (as a sixth 'astrometric' parameter, a_6) and calculating a mean value for each bin in the colour index $B_T - V_T$. The data were derived by NDAC in a special 30-month solution.*

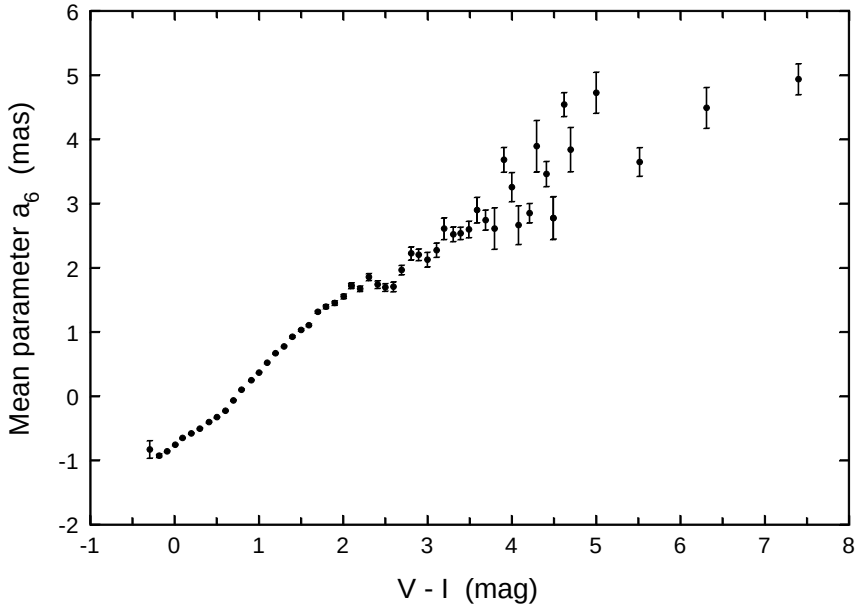

Figure 16.3. *The same as Figure 16.2, but with a_6 binned according to colour index $V - I$.*

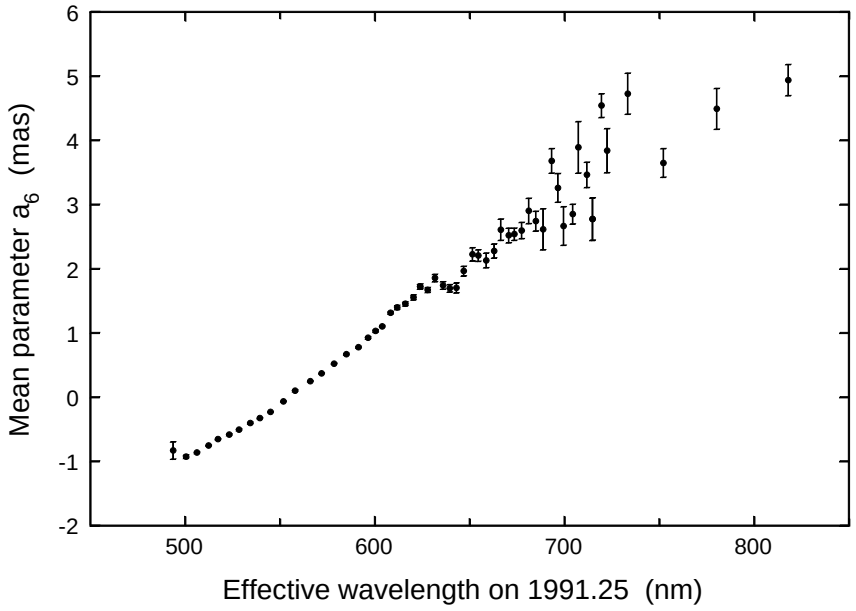

Figure 16.4. *The same as Figure 16.2, but with a_6 binned according to the effective wavelength at epoch J1991.25.*

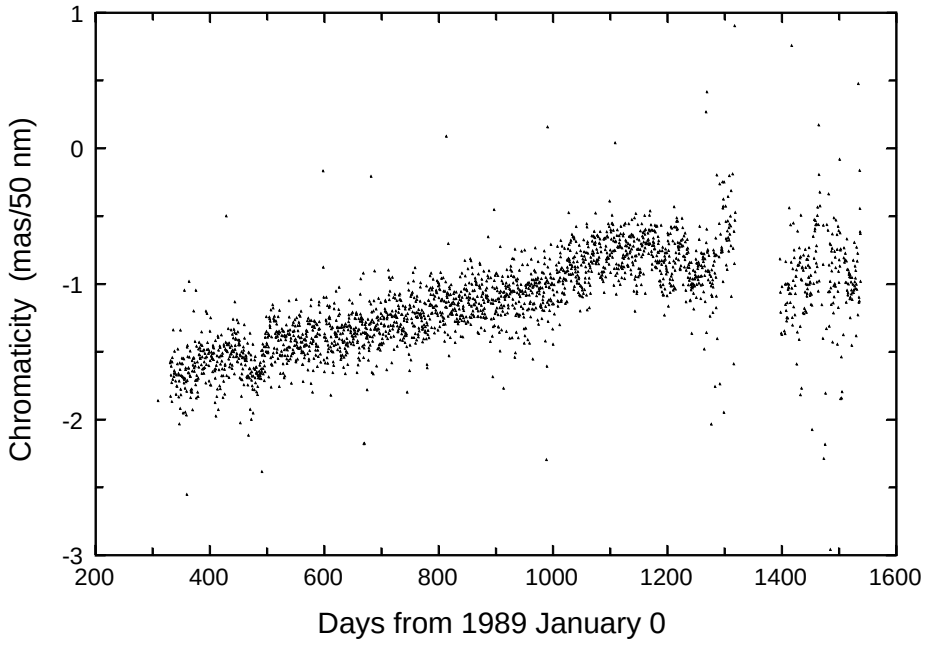

Figure 16.5. *Evolution of chromaticity (Q_N) determined independently for each great-circle reduction, i.e. as a function of the orbit number, N. The data were derived by NDAC in a preliminary 37-month solution.*

16.4. FAST Sphere Solutions

Overall Organisation

Unlike NDAC, the sphere solution and the determination of the astrometric parameters were considered as two different tasks in the data reduction scheme adopted by FAST (see Chapter 11).

In the first step a sphere solution was computed from the reduction on the circles to bring all the abscissae of the subset of stars referred to as the primary reference stars into the same reference system. Up to this point the abscissae had been constructed with a set of inconsistent origins on the circles. The main result of the FAST sphere solution was then a file containing the correction to be applied to each origin, one per circle, so that the resulting network of circles determined a consistent reference frame on the sphere. At the same time several global parameters were computed, such as those connected to the chromaticity and the thermal effects.

The criteria used to select the primary reference stars included the number of abscissae available and the fact that the observations were clean, i.e. the star was not detected to be, or suspected of being, double. Also, a primary reference star had to be photometrically constant, as far as this could be ascertained with the Hipparcos observations. In addition, the distribution of the stars was chosen to achieve a uniform density on the sky with at least one star per square degree. Finally after a first run, all the stars with large correlation coefficients between the astrometric parameters were excluded from the selection, on the ground that this indicated a poor time distribution of the observations.

In the second step, the abscissae of the primary reference stars and of the other programme stars were referred to the new origins and corrected for the global parameters. Then, on a star by star basis, a least-squares fit of the abscissae was made for the five astrometric parameters $\Delta\lambda*$, $\Delta\beta$, $\Delta\pi$, $\Delta\mu_{\lambda*}$, $\Delta\mu_{\beta}$. The remaining grid-step errors were searched for in this step and removed accordingly. For the double and multiple stars a similar procedure was applied for the photocentre or the primary, according to the separation, by correcting the abscissae as explained in Chapter 13.

Iterations

After every run, corresponding to a sphere solution and an astrometric solution for all the stars, an improved astrometric catalogue was made available, at least for the stars with an accepted solution. This new version of the catalogue was virtually free of grid-step errors and much closer to the true position on the sky than the Input Catalogue. In the iterative mode, advantage was taken of the good knowledge of the along-scan attitude to improve, with the star-mapper data, the two transverse attitude angles (see Chapter 7). Then, from the improved attitude and the new reference catalogue, an update was made of the residual between the observed and computed abscissae of the reference great circles already processed before the iteration. The same reference catalogue was used also for the processing of subsequent observations not yet considered.

This procedure led to the computation of several solutions as more data were made available. The main characteristics of these solutions regarding the duration, number of stars and observations are given in Table 16.1. The various iterations over the 37 months are listed in Table 16.2.

Main Features of the Iterated Solutions

The first sphere solution was computed in November 1990 on the 300 reference great circles derived from the first six months of data. This run was used to test the two methods developed within the FAST consortium, to solve the equations of the sphere, on real data. Improved positions were obtained for about 10 000 stars.

F12 and F12R: These two solutions were constructed from a full year of data. They yielded the estimates of the origins of 758 reference great circles. The instrumental effects were represented by seven global parameters for the thermal variations and a single global term for the chromaticity. Thus, with Γ_k denoting the kth global parameter, the abscissa correction of the ith star on the jth circle was written:

$$v_{ji}^{\text{obs}} - v_{ji}^{\text{calc}} = \sum_{k=1}^{8} \frac{\partial v_{ji}}{\partial \Gamma_k} \Gamma_k \qquad [16.12]$$

with the partial derivatives:

$$\frac{\partial v_{ji}}{\partial \Gamma_k} = \cos n(v_{ji} - v_{j\odot}), \quad \text{with } n = 1, 2, 3, 6 \text{ for } k = 1, 2, 4, 6 \qquad [16.13]$$

$$\frac{\partial v_{ji}}{\partial \Gamma_k} = \sin n(v_{ji} - v_{j\odot}), \quad \text{with } n = 2, 3, 6 \text{ for } k = 3, 5, 7 \qquad [16.14]$$

for the thermal variations, and:

$$\frac{\partial v_{ji}}{\partial \Gamma_8} = (B - V)_i - 0.5 \qquad [16.15]$$

for the chromatic term. In these equations v_{ji} is the abscissa of the ith star and $v_{j\odot}$ that of the Sun. The values of the coefficients Γ_k found in the different iterations are given in Table 16.3. The meaning of the coefficients evolved somewhat during the processing as the instrument modelling was refined.

The version F12 of the solutions included the five astrometric parameters for 30 411 stars. However the time base of 12 months was too short an interval to expect an accurate determination of the proper motions. The run served primarily as a test of all the interfaces. A restricted solution, F12R, was computed by adjusting only the two positional parameters and the parallax, constraining the proper motions to their reference catalogue values. The median formal errors in ecliptic longitude and latitude reached respectively 2.0 and 1.7 mas, and 2.5 mas in the parallax.

F18 and F18.1: These runs were based on about 18 months of data covering the observations from the beginning of the mission until 21 June 1991. The instrument modelling was the same as for the 12 months solution. The amplitudes of the thermal terms were all less than one milliarcsec. Only the chromatic term brought a significant contribution to the abscissae with an amplitude larger than 1 mas/mag. The abscissa origins could be determined with a precision better than 0.2 mas and ranged within 5–10 mas from the arbitrary origins set by the great-circle solutions. F18.1 was the first iterated solution using both a new reference catalogue and the attitude software in iterated mode. The gain in precision for the astrometric parameters was between 6 and

9 per cent as shown in Figure 16.6, where the dashed lines refer to the solution before iteration. The activation of the attitude in iterated mode was the only significant change between F18 and F18.1.

F30: All observations up to 6 June 1992 were used to build the 30-month solution leading to 1914 reference great circles. For the first 18 months the attitude and abscissae were not recomputed but were taken from F18.1. For the remaining data a non-iterated mode was used for the attitude and F18 was the reference catalogue. A new model for the chromaticity was introduced which changed the meaning of the parameters Γ_6, Γ_7 and Γ_8 (Table 16.3), which were now defined as:

$$\frac{\partial \nu_{ji}}{\partial \Gamma_6} = (V-I)_i - 0.5 \qquad [16.16]$$

$$\frac{\partial \nu_{ji}}{\partial \Gamma_7} = [(V-I)_i - 0.5]^2 \qquad [16.17]$$

$$\frac{\partial \nu_{ji}}{\partial \Gamma_8} = [(V-I)_i - 0.5](T_j - T_0) \qquad [16.18]$$

where T_0 = J1990.75 was the reference epoch for these solutions. Note that the colour index used was $V-I$ instead of $B-V$. In Figure 16.8, which shows the corrections to the abscissa origins as a function of time, the difference in quality between the circles in iterated mode and those in nominal mode (from day 902) is evident. The astrometric precision improved, as expected, more or less as $t^{-1/2}$ for the positions and parallax and as $t^{-3/2}$ for the components of the proper motion.

F37, F37.1, F37.3: The nominal processing of the observations acquired later than 20 April 1991 was done with the F18 reference catalogue. The 18-month abscissae and attitude were kept and a new catalogue F37 was produced at the end of this processing, with the same instrument modelling as in F30.

An iterated solution was computed with all the available data, including the observations carried out in sun-pointing mode. This resulted in 2269 reference great circles and an astrometric solution (F37.1) for all the stars, single as well as double.

The very last iteration in FAST led to the catalogue F37.3 which was used as the FAST solution for the merging (Chapter 17). The instrument modelling with the global parameters was kept unchanged. However, in addition to the origin of each great circle, a function $C_j \cos 6(\nu - \nu_\odot) + S_j \sin 6(\nu - \nu_\odot)$ was determined to account for a possible systematic resonance between the basic angle and 360°. The amplitudes found in the FAST solutions were very similar to NDAC's with C_j, $S_j \simeq 2$ mas, although for a few great circles the amplitude was as large as 10 mas. The mean and rms abscissa residuals over each reference great circle are shown in Figures 16.9–16.10. The marked change in the dispersion of the residuals at about day 600 followed a modification in the time allocation strategy at the grid level.

The final precision is shown in Figure 16.7 as a function of the ecliptic longitude. For the sake of comparison, the F30 solutions are shown in dashed lines. As expected the improvement was particularly noticeable in proper motion because of the longer time base. This solution included the astrometric parameters for 16 180 double stars of which 10 220 were computed for the brighter component while for the 5960 close binaries with separation $\varrho < 0.35$ arcsec the astrometric solution referred to the photocentre. The typical precisions of the solutions, for single and double stars are given in Table 16.4.

Gravitational Deflection

The FAST sphere solutions described above did not include a global parameter corresponding to a correction to the general-relativistic light deflection. The observation equations were instead corrected in accordance with General Relativity, i.e. assuming the nominal value for the PPN parameter, $\gamma = 1$. However, several special runs of the 37-month solution were made in which this parameter was treated as a global parameter (see Equation 11.19). The runs differed in the modelling of other global parameters and the selection of stars and reference great circles, but they all produced results consistent with the General Relativistic value of $\gamma = 1$ to within the standard errors of the solutions. The net result of these experiments can be summarised as:

$$\gamma = 1.000 \pm 0.004 \qquad [16.19]$$

but with non-negligible correlations with the parallaxes and several other global parameters.

16.5. Evolution of Standard Errors

The standard errors in position were generally different in right ascension and declination: in fact, the error ellipses tended to be oriented along the ecliptic axes due to the symmetry of the scanning law with respect to the ecliptic plane. The situation was similar for the standard errors in the proper motion components. When considering the global precision of the solutions, it is convenient to neglect the anisotropy of the uncertainty and adopt the rms values

$$\sigma_{\rm pos} = \sqrt{\frac{\sigma_{\alpha*}^2 + \sigma_\delta^2}{2}} \qquad \text{and} \qquad \sigma_\mu = \sqrt{\frac{\sigma_{\mu_{\alpha*}}^2 + \sigma_{\mu_\delta}^2}{2}} \qquad [16.20]$$

as representative of the standard errors in position and proper motion for any given star. These quantities are invariant with respect to the coordinate system used. σ_μ should not be confused with the standard error of the modulus of the proper motion.

The evolution of the standard errors of the NDAC, FAST and merged solutions are illustrated in subsequent figures and tables. Only stars in common with the 'basic subset' defined in Section 16.2 are included in the statistics.

NDAC and FAST Solutions

The distributions of the formal standard errors of the astrometric parameters are shown in Figures 16.11–16.13 for NDAC, and in Figures 16.15–16.17 for FAST. In each diagram the distributions are compared with that of the final Hipparcos Catalogue. The 10th, 50th and 90th percentiles of the distributions are given in Tables 16.5 and 16.6. The positions refer to the mean effective catalogue epochs $\langle T_{\rm eff} \rangle$ also given in the tables; these were obtained as the median values of the individual effective epochs calculated by Equation 1.2.10 of Volume 1.

Table 16.2. History of the FAST processing with attitude in the initial mode (label 0) or with the iterated mode according to the iteration level (labels 1, 2, 3). For example the solution over 30 months was constructed with the F18 catalogue as reference data, and resulted in the catalogue F30. The first 18 months included the improved attitude using the F18 positions and the along-scan angle derived with the F18 abscissae, while the observations between 18 and 30 months were processed in the initial mode directly from the star mapper attitude. HIC = Hipparcos Input Catalogue.

Reference catalogue	Output catalogue	Months 6	12	18	30	37
HIC	F12	0	0			
HIC	F18	0	0	0		
F18	F18.1	1	1	1		
F18	F30	1	1	1	0	
F18	F37	1	1	1	0	0
F37	F37.1	2	2	2	1	1
F37.1	F37.3	3	3	3	2	2

Table 16.3. Values of the global parameters in the FAST solutions. The instrument model changed between the 18-month and 30-month solutions.

	Γ_1	Γ_2	Γ_3	Γ_4	Γ_5	Γ_6	Γ_7	Γ_8
	mas	mas	mas	mas	mas	mas	mas	mas/mag
F12R	−0.0082	+0.0146	−0.0838	+0.2833	+0.4379	+0.4877	−0.4260	−2.1491
F18.1	+0.0270	−0.0104	−0.0293	−0.0221	−0.0363	+0.0506	−0.0286	−1.5971
	mas	mas	mas	mas	mas	mas/mag	mas/mag^2	mas/mag/yr
F30	+0.0075	+0.0004	+0.0034	−0.0031	−0.0065	−0.3906	+0.0843	+0.3764
F37.3	+0.0080	−0.0050	+0.0098	−0.0038	−0.0031	−0.3221	+0.1226	−0.0622

Table 16.4. Mean precision of the astrometric parameters for a star of magnitude $Hp = 8$. For double stars separate statistics are given for close systems (separation $\varrho < 0.35$ arcsec), for which the astrometric parameters of the photocentre were derived, and wider systems where the solution referred to the primary component.

Parameter	Single stars	Double stars photocentre	primary	Unit
$\lambda*$ ($= \lambda \cos\beta$)	0.8	1.0	1.8	mas
β	0.7	0.8	1.5	mas
π	1.0	1.4	2.2	mas
$\mu_{\lambda*}$	1.0	1.3	2.2	mas/yr
μ_β	0.8	1.1	1.8	mas/yr

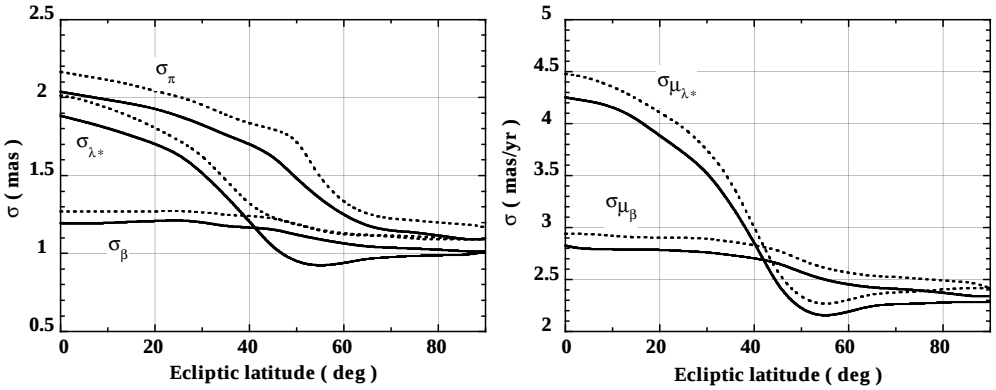

Figure 16.6. *Mean precision of the FAST 18-month solutions as function of ecliptic latitude. Dashed line: non-iterated solution (F18); continuous line: iterated solution (F18.1).*

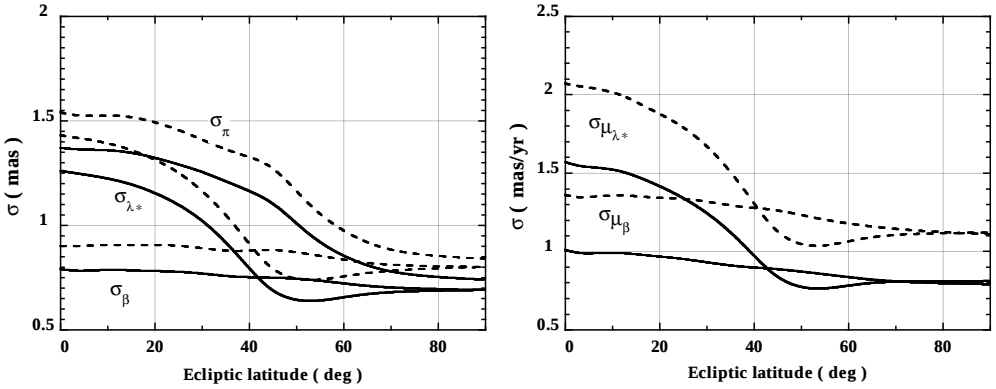

Figure 16.7. *Mean precision of the FAST 30- and 37-month solutions as function of ecliptic latitude. Dashed line: 30-month solution (F30); continuous line: the final, iterated 37-month solution (F37.3).*

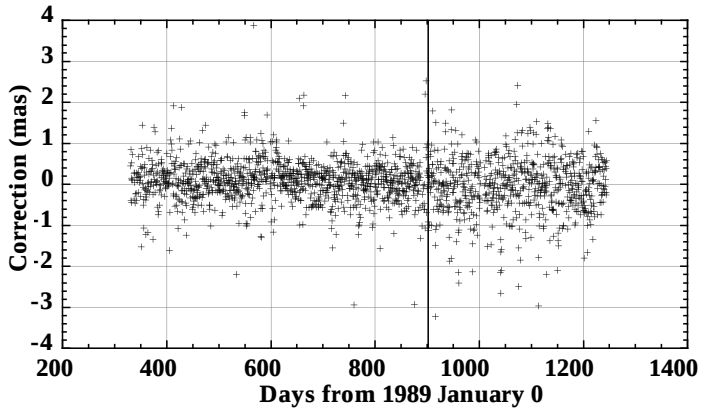

Figure 16.8. *Correction to the a priori origins of the circles obtained in the solution F30. The attitude of the first 18 months (up to day 902) was determined with the iterated mode while the rest used standard processing.*

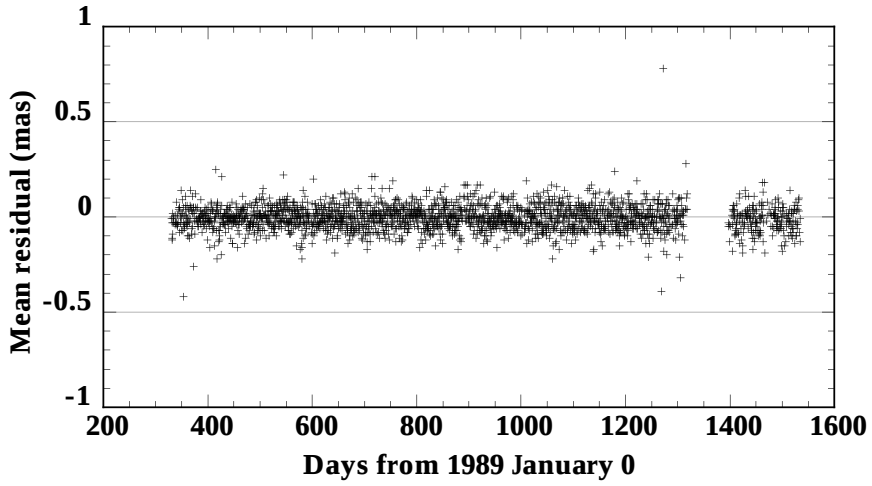

Figure 16.9. *Mean residual of the abscissae of the final FAST solution (F37.3) as a function of time. Each data point corresponds to a single circle.*

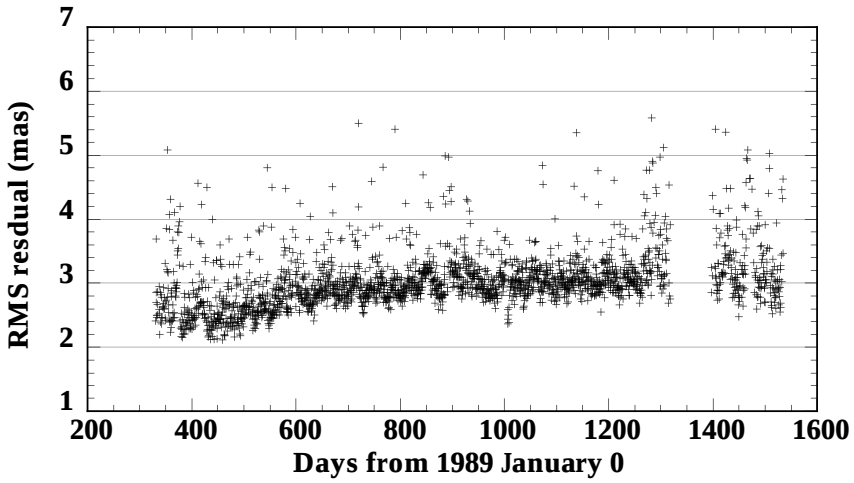

Figure 16.10. *Root mean square residual of the abscissae of the final FAST solution (F37.3) as a function of time. Each data point corresponds to a single circle.*

Table 16.5. Summary of formal standard errors in the successive NDAC sphere solutions, for stars in common with the 'basic subset' of the final catalogue ($\simeq$ single or at least unproblematic stars). The number of stars included in the statistics is given in the second column. The typical range of standard errors is given in the form of the 10th and 90th percentiles, i.e. the values below which 10 and 90 per cent of the standard errors fall. The typical standard error is given by the median value, or 50th percentile. σ_π is the standard error in parallax; $\sigma_{\rm pos}$ and σ_μ are the standard errors in position and proper motion, defined by Equation 16.20. The standard errors in position refer to the epoch in the first column, which is close to the mean epoch of observation for the data considered.

Solution Epoch	No. of stars	Standard error	Percentiles 10%	50%	90%	Unit
N0R	13 887	σ_π	1.64	3.67	14.94	mas
1990.40		$\sigma_{\rm pos}$	1.31	3.00	11.35	mas
N12	43 053	σ_π	1.51	2.10	3.03	mas
1990.40		$\sigma_{\rm pos}$	1.20	1.56	2.30	mas
		σ_μ	3.96	5.24	7.60	mas/yr
N12R	75 919	σ_π	1.52	2.18	2.76	mas
1990.40		$\sigma_{\rm pos}$	1.20	1.61	2.13	mas
N18	94 210	σ_π	1.34	1.98	2.79	mas
1990.70		$\sigma_{\rm pos}$	1.05	1.47	2.15	mas
		σ_μ	2.37	3.35	5.06	mas/yr
N30	96 881	σ_π	1.05	1.54	2.12	mas
1991.15		$\sigma_{\rm pos}$	0.82	1.13	1.59	mas
		σ_μ	1.13	1.60	2.34	mas/yr
N37.1	100 717	σ_π	1.00	1.49	2.09	mas
1991.25		$\sigma_{\rm pos}$	0.78	1.08	1.56	mas
		σ_μ	0.90	1.29	1.99	mas/yr
N37.5	101 071	σ_π	0.85	1.27	1.92	mas
1991.25		$\sigma_{\rm pos}$	0.64	0.93	1.42	mas
		σ_μ	0.74	1.11	1.81	mas/yr

The standard errors shown in these figures and tables depend on the *a priori* weights assigned to the input data. For instance, a re-evaluation of the weights between solutions N37.1 and N37.5 accounts for most of the apparent improvement between these two solutions. The actual improvement of the successive solutions may however be appreciated from the distributions of the parallax values, and in particular the tail of negative values, which resembles the distribution of true errors. These distributions are shown in Figures 16.14 and 16.18, again with the final catalogue included for comparison.

The temporal evolution of the median standard errors and fraction of negative parallaxes is summarised in Figures 16.19–16.22. The positions and parallaxes improve, as expected, roughly as $t^{-1/2}$, if t is the total duration of the observations, and the proper motions slightly slower than $t^{-3/2}$. Empirically, the fraction of negative parallaxes improves roughly as $t^{-1.0}$.

Table 16.6. Summary of formal standard errors in the successive FAST sphere solutions, for stars in common with the 'basic subset' of the final catalogue. See Table 16.5 for further explanation.

Solution Epoch	No. of stars	Standard error	Percentiles 10%	50%	90%	Unit
F12	30 411	σ_π	3.66	6.24	10.91	mas
1990.40		σ_{pos}	2.81	5.10	9.50	mas
		σ_μ	2.93	4.96	8.20	mas/yr
F12R	44 756	σ_π	1.38	2.33	3.44	mas
1990.40		σ_{pos}	1.07	1.72	2.56	mas
F18	88 922	σ_π	1.08	1.79	2.90	mas
1990.70		σ_{pos}	0.84	1.34	2.21	mas
		σ_μ	1.91	3.07	5.20	mas/yr
F18.1	89 040	σ_π	1.23	1.71	2.55	mas
1990.70		σ_{pos}	0.88	1.27	1.96	mas
		σ_μ	2.03	2.95	4.65	mas/yr
F30	95 025	σ_π	0.89	1.34	1.93	mas
1991.15		σ_{pos}	0.69	0.98	1.43	mas
		σ_μ	0.98	1.42	2.16	mas/yr
F37.1	101 222	σ_π	0.87	1.32	1.95	mas
1991.25		σ_{pos}	0.67	0.96	1.45	mas
		σ_μ	0.79	1.16	1.85	mas/yr
F37.3	101 189	σ_π	0.85	1.30	2.02	mas
1991.25		σ_{pos}	0.65	0.95	1.50	mas
		σ_μ	0.76	1.15	1.92	mas/yr

Table 16.7. Summary of formal standard errors in the merged solutions H18, H30 and HIP (the final Hipparcos Catalogue), for stars in common with the 'basic subset' of the final catalogue. See Table 16.5 for further explanation. Detailed statistics for the whole Hipparcos Catalogue are found in Volume 1, Part 3.

Solution Epoch	No. of stars	Standard error	Percentiles 10%	50%	90%	Unit
H18	96 692	σ_π	1.24	1.87	2.71	mas
1990.70		σ_{pos}	0.97	1.39	2.09	mas
		σ_μ	2.23	3.20	4.99	mas/yr
H30	100 293	σ_π	0.97	1.44	2.03	mas
1991.15		σ_{pos}	0.76	1.06	1.51	mas
		σ_μ	1.06	1.51	2.26	mas/yr
HIP	101 246	σ_π	0.71	1.06	1.62	mas
1991.25		σ_{pos}	0.53	0.77	1.19	mas
		σ_μ	0.61	0.91	1.49	mas/yr

Merged Solutions

Table 16.7 summarises the standard errors in the catalogues obtained by merging (combining) the FAST and NDAC sphere solutions. H18 and H30 are provisional catalogues constructed from the 18 and 30-month solutions, while HIP designates the final

Hipparcos Catalogue. The merging technique used for the final catalogue is described in detail in Chapter 17; briefly, it combines the intermediate abscissa results from the two consortia into new solutions for the astrometric parameters, taking into account the estimated correlations between the two data sets. The resulting standard errors reflect the improvement expected from the combination of data which are only partially correlated.

In contrast to the elaborate merging of the final data, H18 and H30 were constructed by simple averaging of the astrometric parameters and covariance matrices. Equal weight was given to the contributing solutions: N18 and F18.1 for H18, and N30 and F30 for H30. Data for stars found in only one of the contributing solutions were directly copied to the merged catalogues, which therefore contain the union of the entries solved by NDAC and FAST. The following transformations were made before the merging:

- the FAST results, including the covariance matrices of the astrometric parameters, were transformed from ecliptic to equatorial coordinates (Volume 1, Section 1.5);
- the NDAC results, including the covariance matrices, were transformed to the epochs adopted for the merged catalogues (J1990.75 for H18, J1991.25 for H30—the FAST solutions already referred to these epochs);
- each contributing solution was transformed to a common reference frame by application of suitable corrections to the orientation and spin of their coordinate systems. Since the final, extragalactic reference frame (Chapter 18) was not yet available, the common reference frame was chosen to be approximately aligned with the FK5 catalogue.

No mean result was computed when the two contributing solutions differed by more than 60 mas in position. This happened for 22 stars in N18/F18.1, and for only one star in N30/F30. After removal of these stars, no gross inconsistencies were found in parallax or proper motion.

16.6. Intercomparisons

The comparison of successive sphere solutions in terms of random and systematic differences has been one of the most important means of checking the reduction procedures and ascertaining the quality of the final catalogue. This section gives an overview of the rather extensive investigations of the various sphere solutions carried out in the course of the reductions. For uniformity, however, the computation of differences and all their analysis have been made afresh after the completion of the Hipparcos Catalogue, using a single and well-defined set of analysis tools. All comparisons are restricted to intersections with the basic subset introduced in Section 16.2.

Rotation Differences

Before comparison, all solutions were aligned with the Hipparcos Catalogue by applying the orientation and spin differences in Table 16.8. The components of the orientation

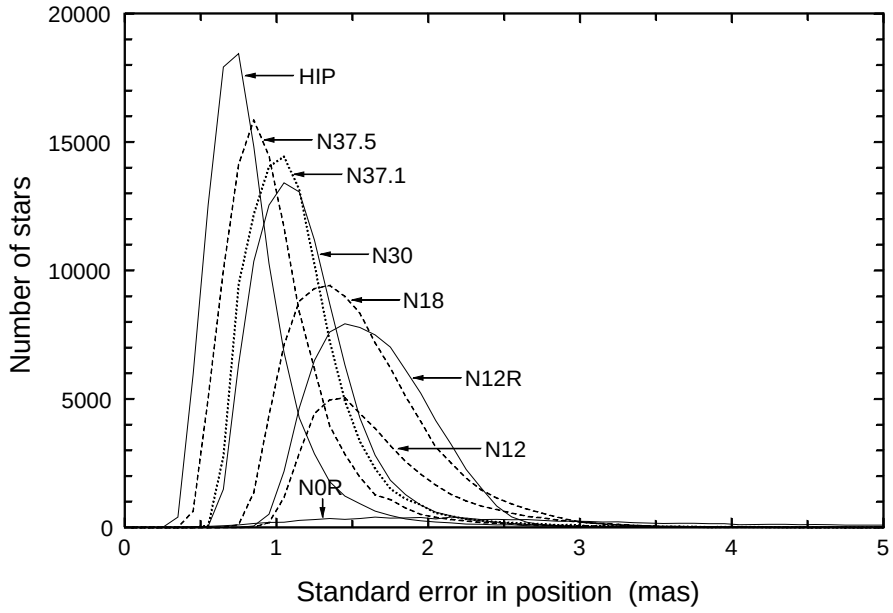

Figure 16.11. *Distribution of formal standard errors in position ($\sigma_{\rm pos}$ in Equation 16.20) for the NDAC sphere solutions (N0R to N37.5) and for the Hipparcos Catalogue (HIP). The data refer to the approximate mean epoch of each solution as given in Table 16.5.*

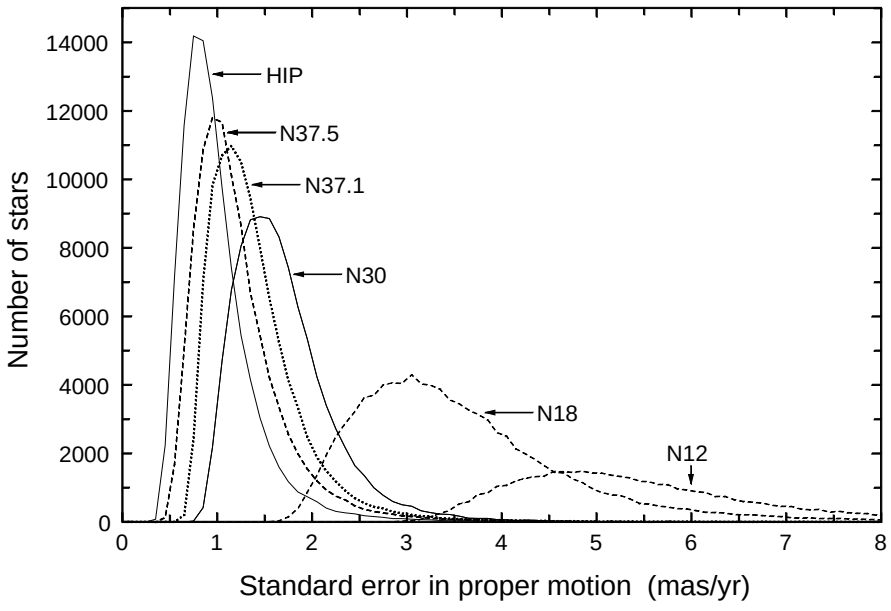

Figure 16.12. *Same as Figure 16.11, but for the standard errors in proper motion (σ_μ in Equation 16.20).*

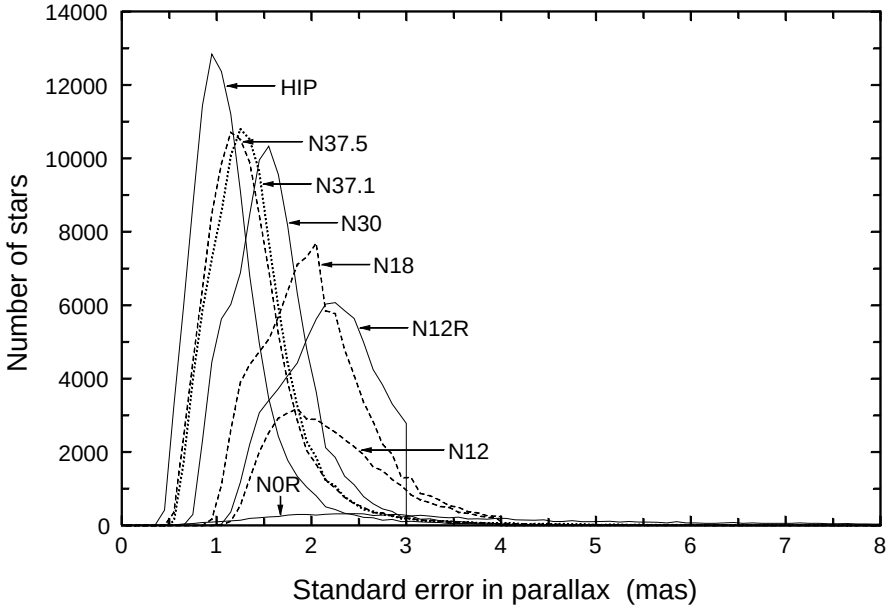

Figure 16.13. *Same as Figure 16.11, but for the standard errors in parallax (σ_π).*

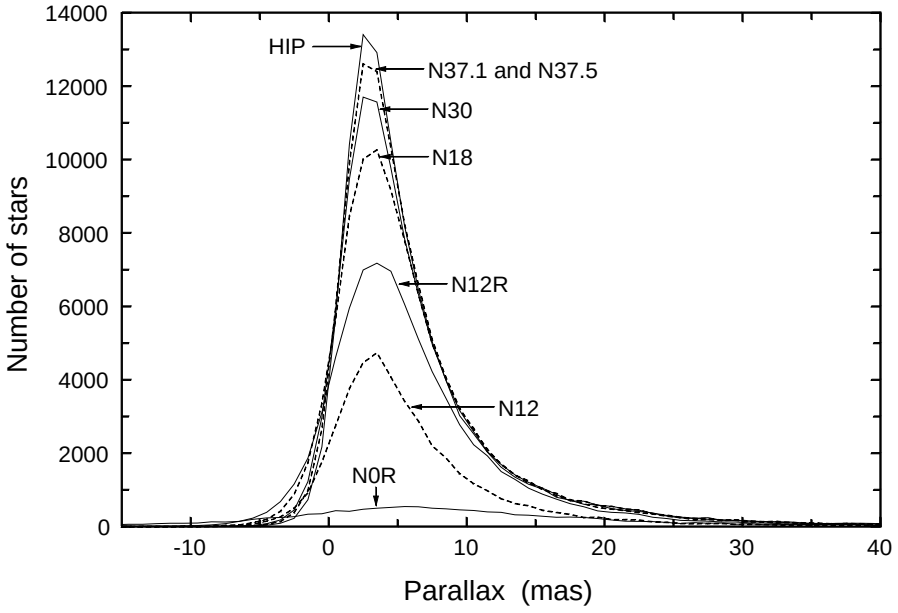

Figure 16.14. *Distribution of parallaxes in the NDAC sphere solutions and the Hipparcos Catalogue. The improvement of the successive solutions can be judged from the height and steepness of the distribution, and from the tail of negative parallax values.*

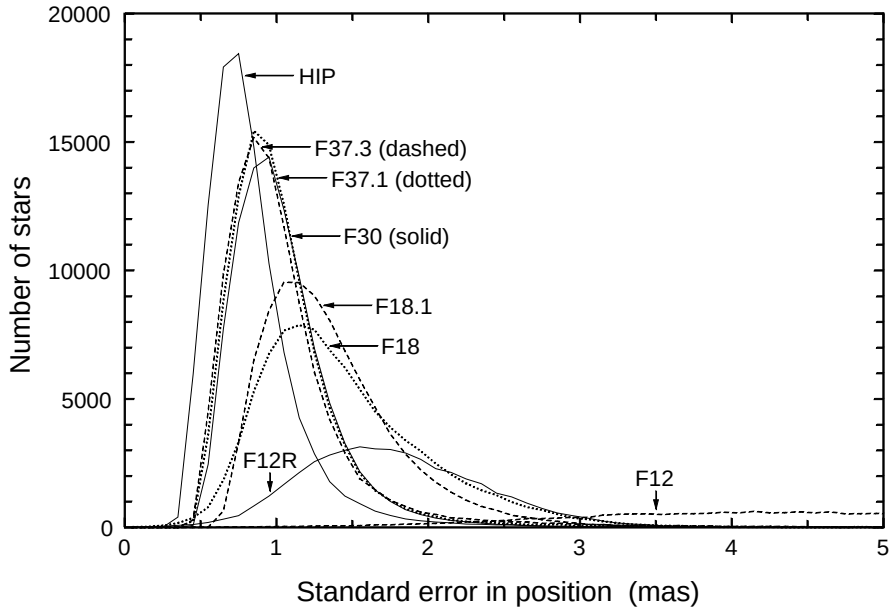

Figure 16.15. *Distribution of formal standard errors in position ($\sigma_{\rm pos}$ in Equation 16.20) for the FAST sphere solutions (F12 to F37.3) and for the Hipparcos Catalogue (HIP). The data refer to the approximate mean epoch of each solution as given in Table 16.6.*

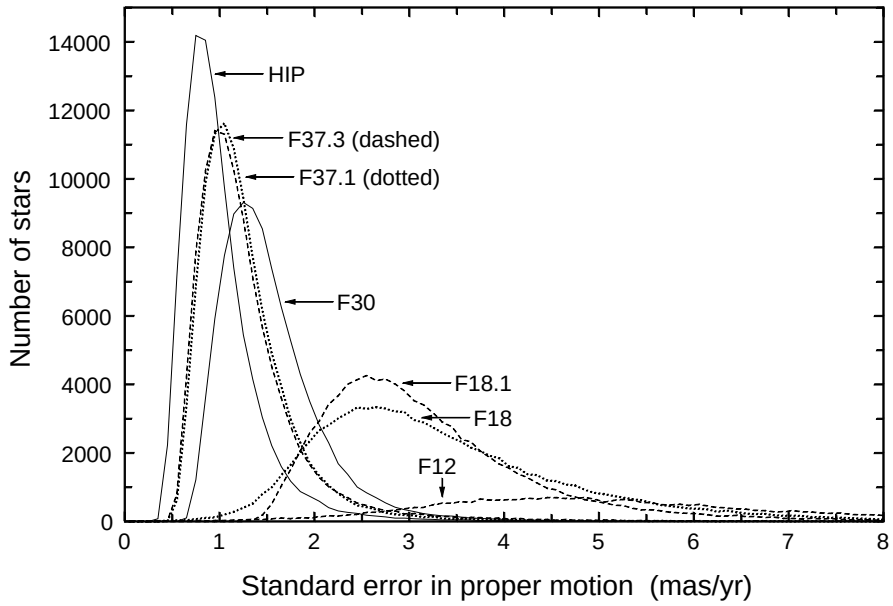

Figure 16.16. *Same as Figure 16.15, but for the standard errors in proper motion (σ_μ in Equation 16.20).*

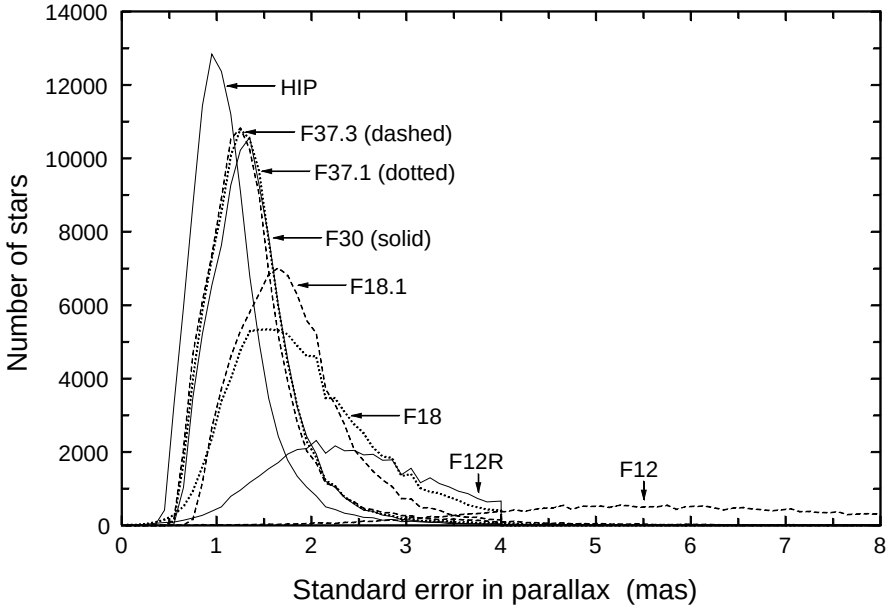

Figure 16.17. *Same as Figure 16.15, but for the standard errors in parallax (σ_π).*

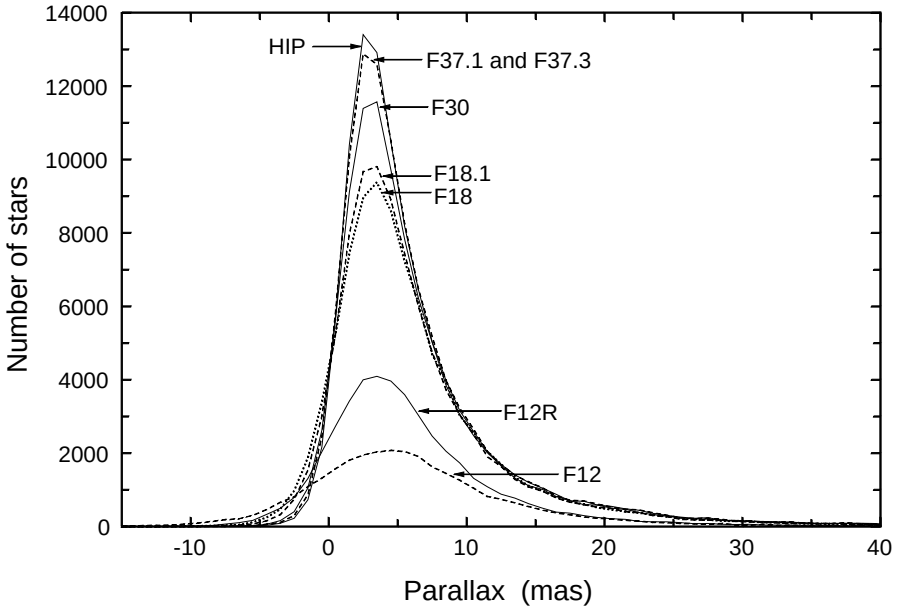

Figure 16.18. *Distribution of parallaxes in the FAST sphere solutions and the Hipparcos Catalogue. The improvement of the successive solutions can be judged from the height and steepness of the distribution, and from the tail of negative parallax values.*

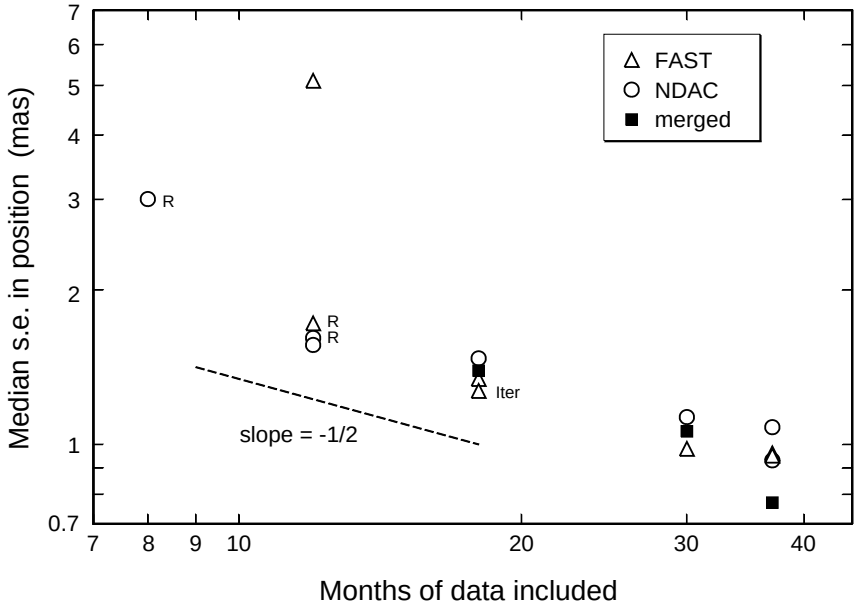

Figure 16.19. *Median standard error in position plotted against the length of the data set included in the solution. A logarithmic scale is used on both axes. The expected improvement as $t^{-1/2}$ is shown by the dashed line. The restricted solutions (no proper motion estimated) are marked 'R'. The FAST iterated 18-months solution (F18.1) is marked 'Iter'.*

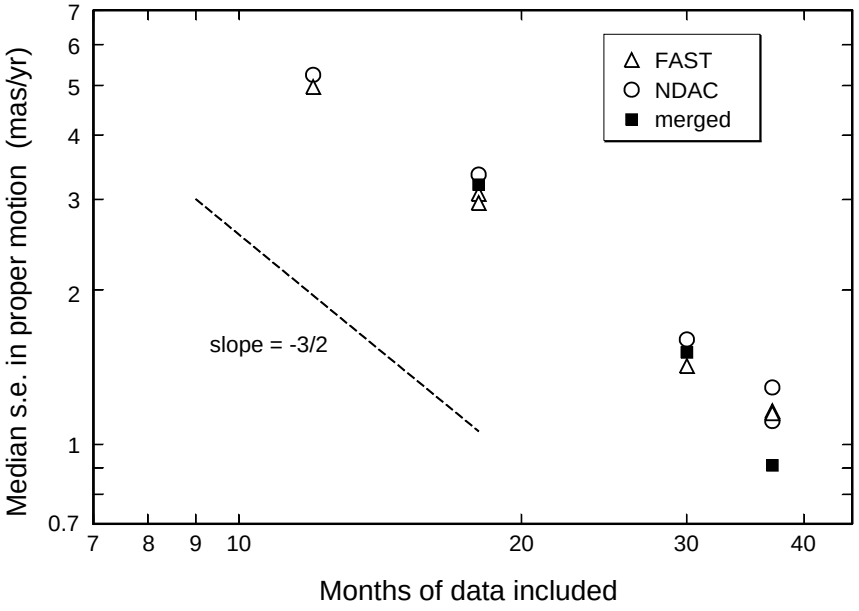

Figure 16.20. *Same as Figure 16.19 but for the standard errors in proper motion. These are expected to improve as $t^{-3/2}$.*

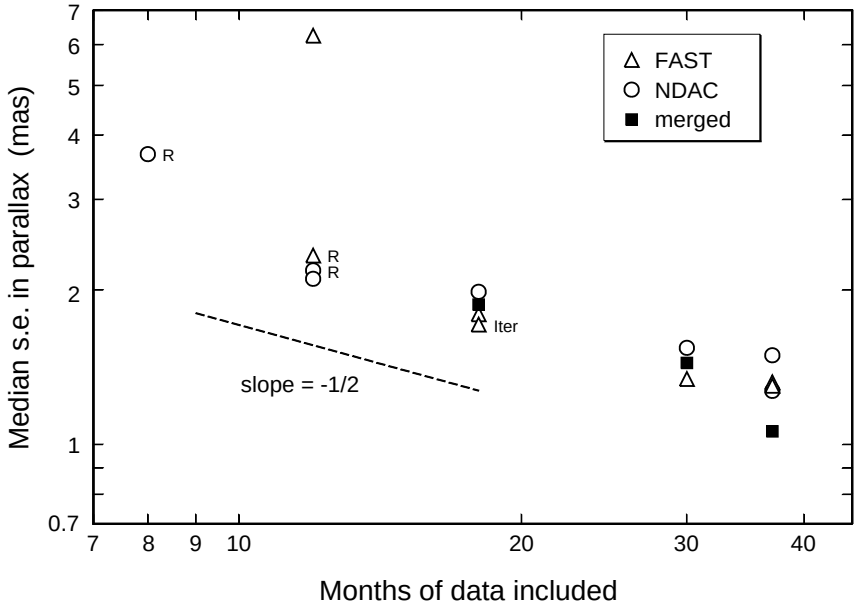

Figure 16.21. *Same as Figure 16.19 but for the standard errors in parallax.*

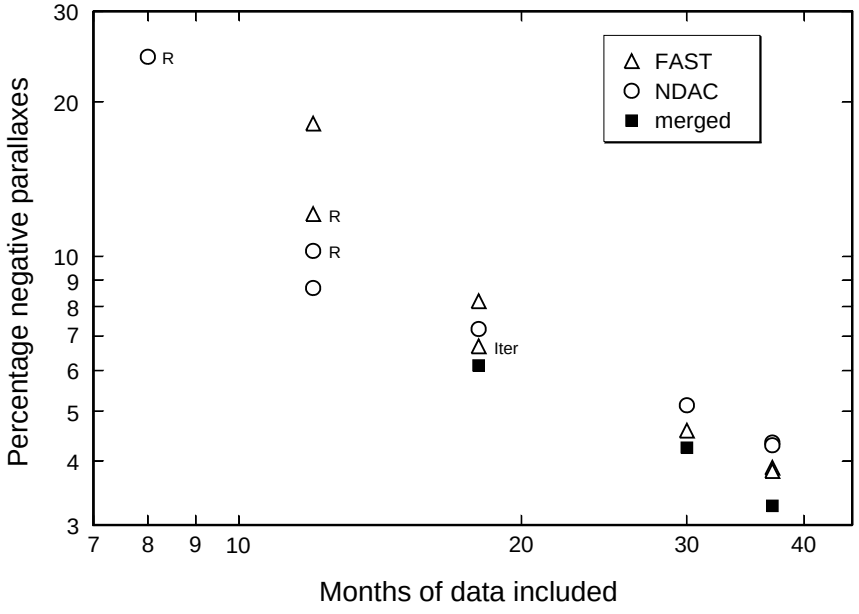

Figure 16.22. *This diagram shows the percentage of negative parallaxes in the various solutions as a function of the length of the data set. Note that the points for the merged catalogues H18, H30 and HIP (filled squares) are significantly below the corresponding points for the FAST and NDAC solutions.*

Table 16.8. Orientation and spin differences between the various sphere solutions and preliminary catalogues, compared with the final Hipparcos Catalogue. See Equation 16.21 for the definition of the orientation differences ($\boldsymbol{\varepsilon}_0$, referred to epoch J1991.25) and spin differences ($\boldsymbol{\omega}$). The last two columns give the mean standard errors of the orientation and spin angles. H37C is the final merged catalogue before it was rotated to the extragalactic reference frame; the orientation and spin parameters in the final row are thus precisely the values adopted for rotating H37C to HIP.

	Orientation (Sol–HIP)			Spin (Sol–HIP)			Standard errors	
Solution (Sol)	ε_{0x} mas	ε_{0y} mas	ε_{0z} mas	ω_x mas/yr	ω_y mas/yr	ω_z mas/yr	σ_ε mas	σ_ω mas/yr
N0R	+17.123	−30.384	+72.228	−0.754	+0.563	+1.362	0.095	0.079
N12	−40.411	−41.606	+67.784	−1.201	+0.974	+1.239	0.026	0.030
N12R	−39.827	−42.139	+67.815	−0.549	+0.253	+1.302	0.027	0.032
N18	−39.937	−41.468	+67.559	−1.235	+0.952	+1.080	0.008	0.012
N30	−39.823	−41.541	+67.565	−1.425	+1.013	+0.968	0.003	0.005
N37.1	−39.904	−41.593	+67.659	−1.335	+0.803	+1.035	0.003	0.003
N37.5	−39.748	−41.651	+67.619	−1.314	+0.707	+0.978	0.002	0.003
F12	−24.615	−30.000	+78.124	−0.012	+1.683	+1.910	0.062	0.079
F12R	−23.949	−22.528	+69.379	−0.516	+0.531	+1.312	0.027	0.034
F18	−24.174	−27.995	+56.402	−0.462	−0.886	+4.109	0.009	0.013
F18.1	−24.029	−29.734	+58.680	−0.567	−3.251	+6.132	0.007	0.011
F30	−24.192	−27.965	+56.493	−0.524	−0.809	+4.013	0.003	0.004
F37.1	−24.201	−27.554	+56.230	−0.582	−0.468	+3.665	0.003	0.003
F37.3	−24.218	−27.532	+56.190	−0.590	−0.453	+3.661	0.002	0.002
H18	−19.351	−9.315	+22.123	−0.704	+0.035	+0.471	0.033	0.010
H30	−19.108	−8.510	+20.914	−0.707	+0.042	+0.473	0.002	0.003
H37C	−19.1	−8.5	+20.9	−0.73	+0.05	+0.47		

and spin differences (ε_{0x}, ε_{0y}, ε_{0z}, ω_x, ω_y, ω_z) were determined by a robust least-squares method, using the following four observation equations for each star in the basic subset:

$$\begin{aligned}
(\alpha_S - \alpha_H)\cos\delta &= -\varepsilon_{0x}\,\sin\delta\cos\alpha - \varepsilon_{0y}\,\sin\delta\sin\alpha + \varepsilon_{0z}\,\cos\delta \\
\delta_S - \delta_H &= +\varepsilon_{0x}\,\sin\alpha - \varepsilon_{0y}\,\cos\alpha \\
(\mu_{\alpha*})_S - (\mu_{\alpha*})_H &= -\omega_x\,\sin\delta\cos\alpha - \omega_y\,\sin\delta\sin\alpha + \omega_z\cos\delta \\
(\mu_\delta)_S - (\mu_\delta)_H &= +\omega_x\,\sin\alpha - \omega_y\,\cos\alpha
\end{aligned} \qquad [16.21]$$

Here, subscripts S and H respectively signify the astrometric parameters in the sphere solution and the Hipparcos Catalogue, always referred to the epoch J1991.25.

Remaining differences in the astrometric parameters were analysed by a variety of methods, with an aim to characterise both the random and the systematic differences between the solutions. The most significant results of this analysis are described hereafter.

Random Differences

For each of the five astrometric parameters, the distributions of the differences between the NDAC and FAST solutions are shown in Figures 16.23–16.27. As a measure of the width of each distribution, a robust 'standard deviation' was computed for each curve; these values are given in Table 16.9. The standard deviations were computed from the

quantiles $x_{\Delta a}(f)$ of the differences, i.e. the values below which a given fraction f of the differences Δa fall. Specifically, the first and fifth sextiles of the distributions were used:

$$\sigma_{\Delta a} = 0.5168 \left[x_{\Delta a}\left(\frac{5}{6}\right) - x_{\Delta a}\left(\frac{1}{6}\right) \right] \qquad [16.22]$$

For a normal distribution this gives the approximate standard deviation. Here, Δa represents the difference in any of the parameters: $\Delta\alpha*$, $\Delta\delta$, $\Delta\pi$, $\Delta\mu_{\alpha*}$, $\Delta\mu_{\delta}$, with the asterisk signifying an implicit $\cos\delta$ factor, and with all differences taken in the sense NDAC minus FAST.

Table 16.10 similarly gives the standard deviations of the differences of each solution with respect to the Hipparcos Catalogue. The overall convergence of the FAST and NDAC solutions towards each other, and towards the final catalogue, is readily seen in these diagrams and tables. Apart from the obvious improvements resulting from the addition of more observations, it is remarkable how the FAST solutions improved by iteration (from F18 to F18.1, and from F37.1 to F37.3; also the NDAC solutions N37.1 to N37.5).

The robust method of Equation 16.22 was introduced because the distributions in Figures 16.23–16.27 are not quite Gaussian: empirically, the far wings tend to decay exponentially, i.e. much slower than for a normal curve. However, even if the errors of each consortium were normal random variables, the distributions in these diagrams could not be expected to be Gaussian, simply because they contain a mixture of populations with different standard deviations. In order to test whether the differences behave normally, they should be scaled by their respective standard errors. Unfortunately the standard errors of the individual differences cannot easily be estimated. As a simple substitute, normalised differences were computed as:

$$\overline{\Delta a} = \frac{a_{\mathrm{N}} - a_{\mathrm{F}}}{\sqrt{\sigma_{a,\mathrm{N}}^2 + \sigma_{a,\mathrm{F}}^2}} \qquad [16.23]$$

where a stands for any of the five astrometric parameters and σ_a for its standard error from the sphere solution. If the standard errors are correctly estimated and not too unequal, then $\overline{\Delta a}$ should be approximately normal with standard deviation $\sqrt{1-\rho}$, where ρ is the correlation between the NDAC and FAST errors.

The distributions of the normalised differences in parallax are shown in Figure 16.28. The standard deviation of $\overline{\Delta\pi}$ decreases from about 0.78 in the early solutions to 0.63 in the final ones, possibly indicating an increased correlation between the consortia solutions. More significant is perhaps the fact that the curves in Figure 16.28 are much more Gaussian-like than in Figure 16.27. Probability plots of $\overline{\Delta\pi}$ (Figure 16.29) show the deviations from normality much more clearly: for the 30-month solutions and for the final solutions these deviations are remarkably small.

Large-Scale Differences

The Hipparcos mission was designed to make global measurements, directly linking widely separated parts of the sky by means of the basic angle of 58°. It is therefore of great interest to see how well different regions of the sky are connected to the mean reference frame defined by all the regions taken together. Some of the extragalactic link data (in particular the VLBI, MERLIN and HST observations; see Chapter 18) provide an external check on possible large-scale distortions of the Hipparcos reference frame,

Table 16.9. Standard deviations of the differences in astrometric parameters between the FAST and NDAC sphere solutions, after each solution had been aligned with the Hipparcos Catalogue by application of the orientation and spin differences in Table 16.8. The second and third columns give the number of stars used in each comparison, and the epoch for the comparison of positions. The standard deviations were computed by the robust method of Equation 16.22.

Solutions compared	No. of stars	Epoch	Standard deviations (mas, mas/yr)				
			$\Delta\alpha*$	$\Delta\delta$	$\Delta\pi$	$\Delta\mu_{\alpha*}$	$\Delta\mu_{\delta}$
N12–F12	39 199	1990.40	3.59	3.19	4.28	11.48	10.30
N12R–F12R	39 199	1990.40	2.09	1.80	2.42	—	—
N18–F18	86 450	1990.70	1.71	1.48	2.09	3.85	3.35
N18–F18.1	86 536	1990.70	1.44	1.26	1.77	3.29	2.86
N30–F30	91 616	1991.15	1.14	0.97	1.35	1.59	1.33
N37.1–F37.1	100 702	1991.25	1.00	0.83	1.19	1.27	1.05
N37.5–F37.3	100 894	1991.25	0.97	0.81	1.17	1.19	0.98

Table 16.10. Standard deviations of the differences in astrometric parameters between the successive sphere solutions and the Hipparcos Catalogue (HIP), after each solution had been aligned with the Hipparcos Catalogue by application of the orientation and spin differences in Table 16.8. The second and third columns give the number of stars used in each comparison, and the epoch for the comparison of positions. The standard deviations were computed by the robust method of Equation 16.22.

Solutions compared	No. of stars	Epoch	Standard deviations (mas, mas/yr)				
			$\Delta\alpha*$	$\Delta\delta$	$\Delta\pi$	$\Delta\mu_{\alpha*}$	$\Delta\mu_{\delta}$
N0R–HIP	13 887	1990.40	7.57	7.70	9.38	—	—
N12–HIP	43 053	1990.40	1.32	1.27	1.95	5.57	5.28
N12R–HIP	75 919	1990.40	1.62	1.44	2.43	—	—
N18–HIP	94 210	1990.70	1.26	1.08	1.69	3.58	3.06
N30–HIP	96 881	1991.15	0.89	0.74	1.09	1.43	1.17
N37.1–HIP	100 717	1991.25	0.70	0.59	0.86	0.94	0.79
N37.5–HIP	101 071	1991.25	0.59	0.49	0.73	0.72	0.60
F12–HIP	30 411	1990.40	3.55	3.15	4.33	10.25	10.24
F12R–HIP	44 756	1990.40	2.13	1.80	2.77	—	—
F18–HIP	88 922	1990.70	1.50	1.29	1.93	3.87	3.40
F18.1–HIP	89 040	1990.70	1.14	0.99	1.54	3.31	2.86
F30–HIP	95 025	1991.15	0.86	0.73	1.01	1.36	1.14
F37.1–HIP	101 222	1991.25	0.57	0.48	0.68	0.70	0.56
F37.3–HIP	101 189	1991.25	0.51	0.43	0.62	0.64	0.51
H18–HIP	96 692	1990.70	1.34	1.25	1.39	3.11	2.66
H30–HIP	100 293	1991.15	0.68	0.57	0.84	1.18	0.97

Table 16.11. North-south asymmetry of the parallax zero points, when comparing the successive FAST and NDAC sphere solutions. The asymmetry $\Delta\pi_0$ is defined by Equation 16.24.

Solutions compared	$\Delta\pi_0$ mas	Solutions compared	$\Delta\pi_0$ mas
N12–F12	+0.461	N30–F30	+0.019
N12R–F12R	+0.142		
N18–F18	−0.005	N37.1–F37.1	+0.015
N18–F18.1	−0.025	N37.5–F37.3	+0.007

but only in very few points. Again, a comparison of successive sphere solutions could however give an idea of the consistency of the data on a large scale.

When comparing the 12-month solutions, a significant difference was noted in the FAST and NDAC parallaxes, depending on ecliptic latitude. The difference could be described as a north-south asymmetry: north of the ecliptic the NDAC parallaxes were systematically larger (by about 0.4–0.5 mas) than the FAST ones, while the opposite was true in the southern sky. This could be understood as an effect of the relative scarcity and weakness of data in the ecliptic region, aggravated by the elliptic satellite orbit causing many more Earth occultations than would have been the case in the nominal orbit. When calculating the parallaxes of stars at high ecliptic latitudes, stars in the ecliptic region served as a reference for the parallax zero point (by having a much smaller parallax factor projected on the reference great circles); if they were absent from the sphere solution, the abscissa zero points may have been shifted to produce systematically different parallaxes in the two hemispheres. The problem was predicted to disappear as more observations accumulated, permitting good solutions also of the stars in the ecliptic region. This was indeed the case (Table 16.11). Defining the parallax asymmetry as:

$$\Delta\pi_0 = \frac{1}{2}\left[\left\langle \pi_N - \pi_F \right\rangle_{\delta>0} - \left\langle \pi_N - \pi_F \right\rangle_{\delta<0}\right] \qquad [16.24]$$

where the angular brackets denote the median value, it was found that the asymmetry decreased to below 0.01 mas in the final solutions.

One rather powerful method of looking for inconsistencies in the system of positions and proper motions is to determine the orientation and spin parameters $\boldsymbol{\varepsilon}_0$ and $\boldsymbol{\omega}$ from only part of the sky, e.g. separately for different hemispheres. Table 16.12 gives the results for the final sphere solutions (N37.5–F37.3), with the sky divided in eight equal parts according to the given intervals in α and δ. (This analysis was made after both solutions had been globally aligned with the Hipparcos Catalogue, so the mean orientation and spin differences over the whole sky are equal to zero.) The largest deviations amount to 0.08 mas in orientation and 0.13 mas/yr in the spin.

Small-Scale Differences

Figures 16.30–16.34 show the differences in the five astrometric parameters, calculated in the sense N37.5–F37.3 and plotted versus position on the sky in colour coding. The spatial resolution of the maps is 2°. At this resolution the differences are typically about ±1.5 mas, but as can be seen from the maps, variations are more pronounced in the ecliptic region where the mean number of observations per star is much smaller than at higher positive or negative ecliptic latitudes (Figure 16.35).

Table 16.12. Orientation and spin differences between the final NDAC and FAST solutions as determined from octants of the sky defined by the given limits in α and δ. The all-sky orientation and spin differences have been removed before the regional differences were calculated. See Equation 16.21 for the definition of the orientation differences ($\boldsymbol{\varepsilon}_0$, referred to epoch J1991.25) and spin differences ($\boldsymbol{\omega}$). The standard errors are typically about 0.012 mas in the orientation components and 0.015 mas/yr in the spin components.

Octant considered		Orientation (N37.5–F37.3)			Spin (N37.5–F37.3)		
α	δ	ε_{0x} mas	ε_{0y} mas	ε_{0z} mas	ω_x mas/yr	ω_y mas/yr	ω_z mas/yr
0–90°	< 0	−0.003	−0.034	−0.046	−0.003	−0.004	−0.029
90–180°	< 0	−0.006	+0.004	+0.002	−0.010	+0.001	+0.004
180–270°	< 0	−0.011	+0.002	+0.078	−0.031	+0.016	+0.125
270–360°	< 0	+0.020	−0.027	−0.049	−0.015	−0.007	+0.003
0–90°	> 0	−0.017	+0.012	−0.024	+0.062	+0.012	+0.070
90–180°	> 0	+0.017	−0.003	−0.011	+0.039	−0.014	−0.025
180–270°	> 0	+0.009	+0.001	+0.016	−0.012	+0.003	+0.004
270–360°	> 0	+0.019	+0.020	+0.006	+0.001	+0.060	−0.097

The angular scale of the differences can be studied more quantitatively by means of the sample correlation function. For any astrometric parameter a, the correlation function is defined in terms of the normalised differences $\overline{\Delta a}$ as:

$$R(\theta) = \frac{\langle\, \overline{\Delta a}_i \, \overline{\Delta a}_j \,\rangle}{\sqrt{\langle\, \overline{\Delta a}_i^2 \,\rangle \, \langle\, \overline{\Delta a}_j^2 \,\rangle}} \qquad [16.25]$$

where the averages are calculated over all pairs of stars (i, j) whose angular separations are in the range $\theta \pm \Delta\theta/2$.

Figure 16.36 shows the sample correlation function for the parallax differences, calculated with a resolution of $\Delta\theta = 0\overset{\circ}{.}1$ by considering all $\simeq 5.09 \times 10^9$ pairs of 100 890 stars common to F37.3, N37.5 and the basic subset. The first few degrees are also shown in Figure 16.37. At angular separations less than a few degrees the correlation is strongly positive, but decreases to almost negligible values for separations greater than $\simeq 4°$. An empirical fit to the first part of the correlation function is given by the function:

$$R(\theta) = R(0) \exp(-0.14\theta - 1.04\theta^2 + 0.41\theta^3 - 0.06\theta^4) \qquad [16.26]$$

where θ is measured in degrees and $R(0) = 0.59$; this function is shown by the solid curve in Figure 16.37. At greater separations (> 4°) the sample correlations are remarkably small, generally on the ±(0.001 to 0.002) level, while there are more significant negative correlations for $\theta \simeq 180°$. Several features of $R(\theta)$ can probably be related to fundamental properties of the great-circle reductions and in particular to the value of the basic angle (58°) and the size of the field of view ($0\overset{\circ}{.}9$). Note for instance the presence of (small but statistically significant) peaks near $\theta = 58°$, $174° = 3 \times 58°$, and $12° = 360° - 6 \times 58°$.

It is likely that the actual parallax errors in the merged catalogue exhibit a similar spatial correlation, but perhaps with a different scale on the vertical axis. For instance, prelaunch simulations of the astrometric errors resulting from the great-circle reductions and sphere solution gave a mean spatial correlation function with a similar initial decrease as in Figure 16.37, but with $R(0) = 0.16$ (Lindegren 1988). Given an assumed shape of the correlation function, e.g. according to the above formula, the normalising factor $R(0)$ may in principle be estimated from the dispersion of parallax values in open clusters.

Table 16.13. Colour dependence of the orientation and spin differences between the NDAC and FAST solutions (see Equation 16.27).

Solutions compared	Colour dependent orientation			Colour dependent spin		
	ε'_{0x}	ε'_{0y}	ε'_{0z}	ω'_x	ω'_y	ω'_z
	mas mag^{-1}			mas yr^{-1} mag^{-1}		
N12–F12	+0.098	−0.400	+0.230	+2.720	+0.834	−0.705
N12R–F12R	+0.130	−0.045	+0.225	—	—	—
N18–F18	−0.006	+0.008	+0.027	−0.670	+0.166	+0.116
N18–F18.1	−0.722	+0.259	−0.009	+0.945	−0.291	+0.141
N30–F30	−0.395	+0.089	−0.008	+0.709	−0.216	−0.048
N37.1–F37.1	+0.045	−0.022	−0.038	−0.064	−0.014	−0.008
N37.5–F37.3	+0.011	−0.016	−0.020	−0.094	+0.020	+0.014

However, for a detailed examination of astrometric correlations in a small area of the sky it is necessary to consider the elementary observations at abscissa level. This is possible by means of the Hipparcos Intermediate Astrometric Data (Volume 1, Section 2.8) and the empirical abscissa correlation functions discussed in Section 17.8.

Colour and Magnitude Effects

In the early sphere solutions it was found that the orientation and spin differences were colour dependent (and perhaps, to a much smaller degree, magnitude dependent). The effect is most clearly seen if the stars are divided in two equal parts according to their colour index or magnitude, and the rotation parameters $\boldsymbol{\varepsilon}_0$ and $\boldsymbol{\omega}$ are determined separately for the two halves. Dividing at $V - I = 0.7$ gives a mean colour index of $\simeq 0.42$ for the bluer half and $\simeq 1.06$ for the redder half. The differences in the rotation parameters divided by the difference in mean colour index (0.64 mag) give the chromatic rotation parameters in Table 16.13:

$$\boldsymbol{\varepsilon}'_0 = \frac{\Delta\boldsymbol{\varepsilon}_0}{\Delta(V-I)}, \qquad \boldsymbol{\omega}' = \frac{\Delta\boldsymbol{\omega}}{\Delta(V-I)} \qquad [16.27]$$

There were very significant colour effects up to and including the 30-month solutions; in the 37-month solutions they are suddenly reduced by an order of magnitude. This drastic improvement is almost entirely due to some change in the FAST solutions between F30 and F37.1, as can be shown by a direct comparison of these two solutions. The explanation appears to be related to the FAST modelling of the chromaticity (Section 16.4), but the actual mechanism is not understood.

A similar division according to magnitude reveals much smaller differences. For the final solutions (N37.5–F37.3) the effect is only marginally significant at ~ 0.007 mas mag^{-1} in orientation and ~ 0.009 mas yr^{-1} mag^{-1} in the spin. The effect could in fact be merely a reflection of the change in mean colour with magnitude.

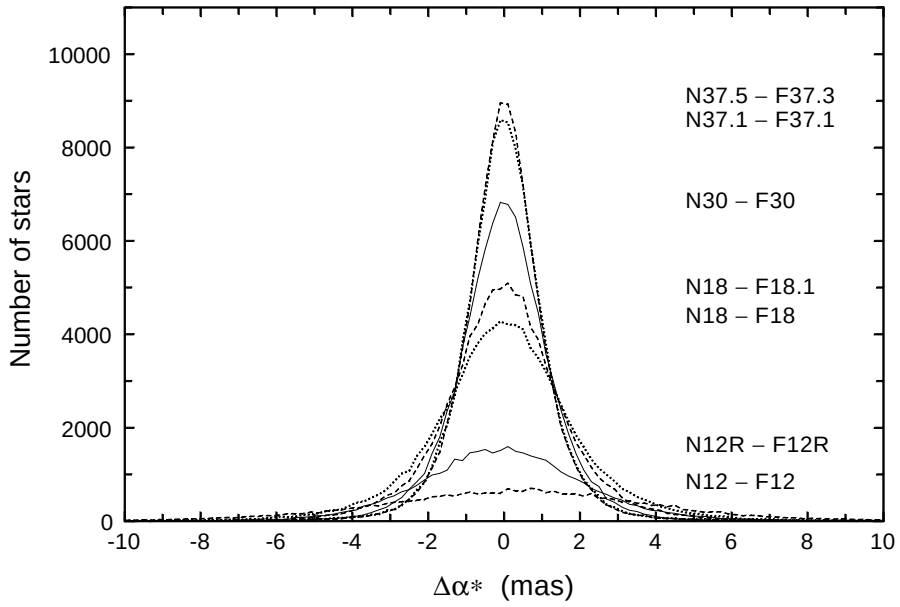

Figure 16.23. *Distributions of the differences in right ascension ($\Delta\alpha* = \Delta\alpha \cos\delta$) between the NDAC and FAST solutions. In this and subsequent figures, the curves may be identified by means of the labels printed at the level of each peak.*

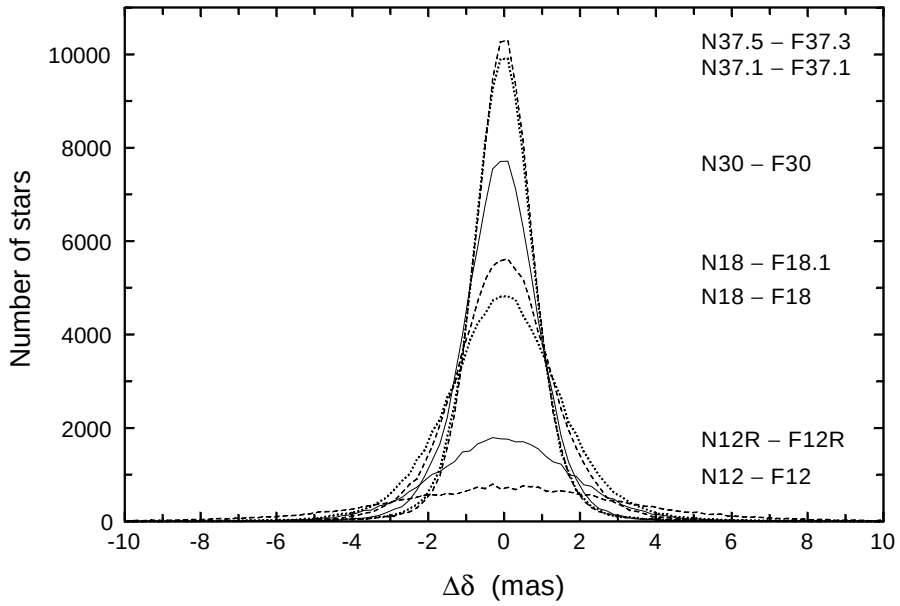

Figure 16.24. *Distributions of the differences in declination between the NDAC and FAST solutions.*

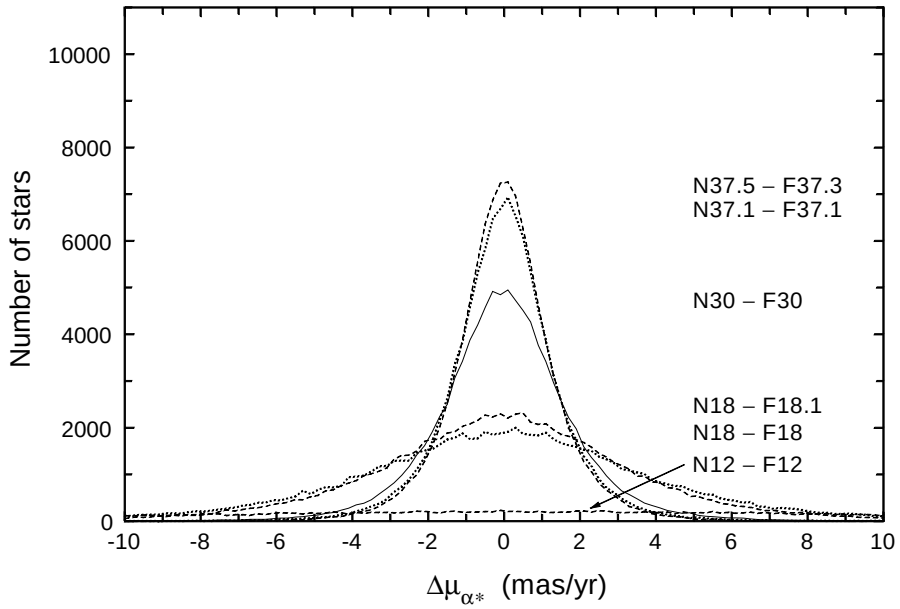

Figure 16.25. *Distributions of the proper motion differences in right ascension ($\Delta\mu_{\alpha*} = \Delta\mu_\alpha \cos\delta$) between the NDAC and FAST solutions.*

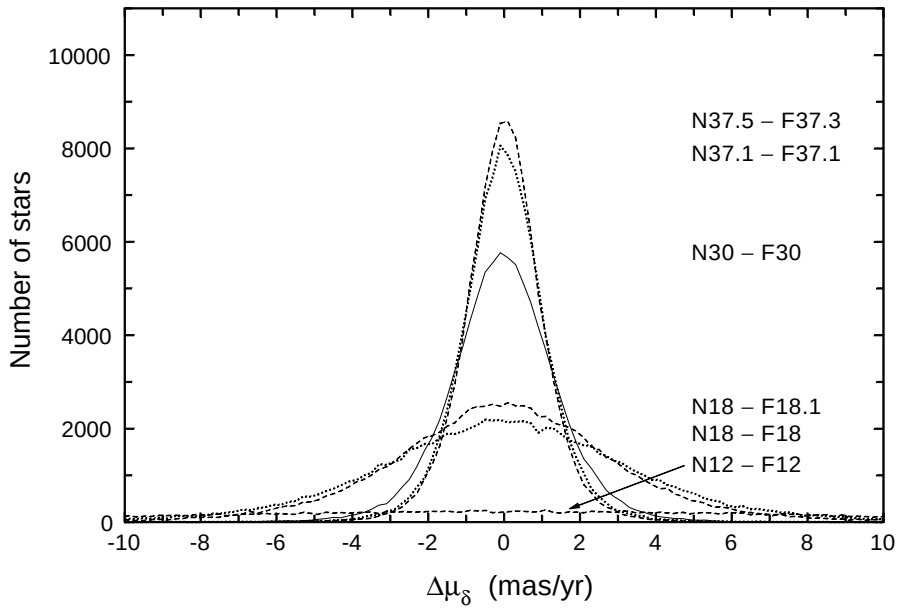

Figure 16.26. *Distributions of the proper motion differences in declination between the NDAC and FAST solutions.*

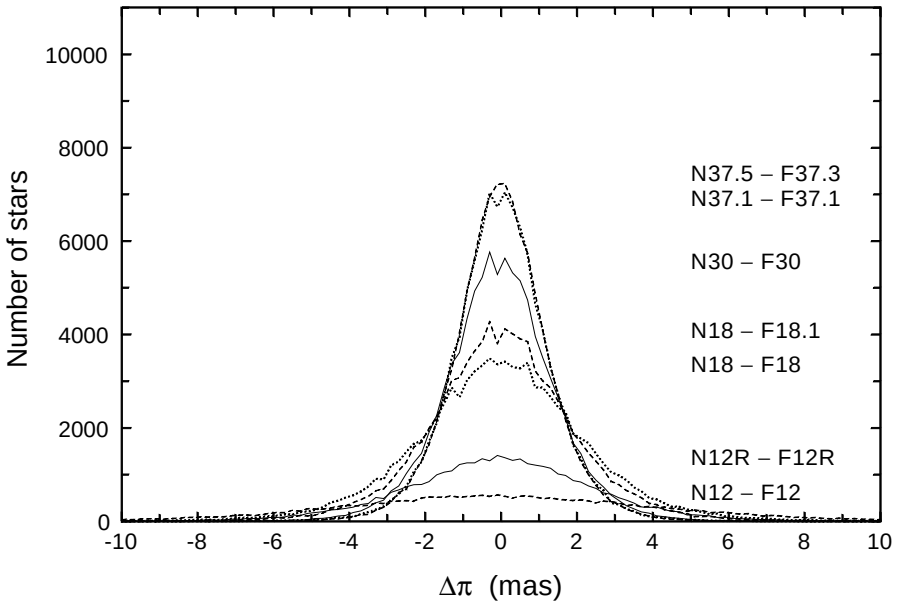

Figure 16.27. *Distributions of the differences in parallax between the NDAC and FAST solutions.*

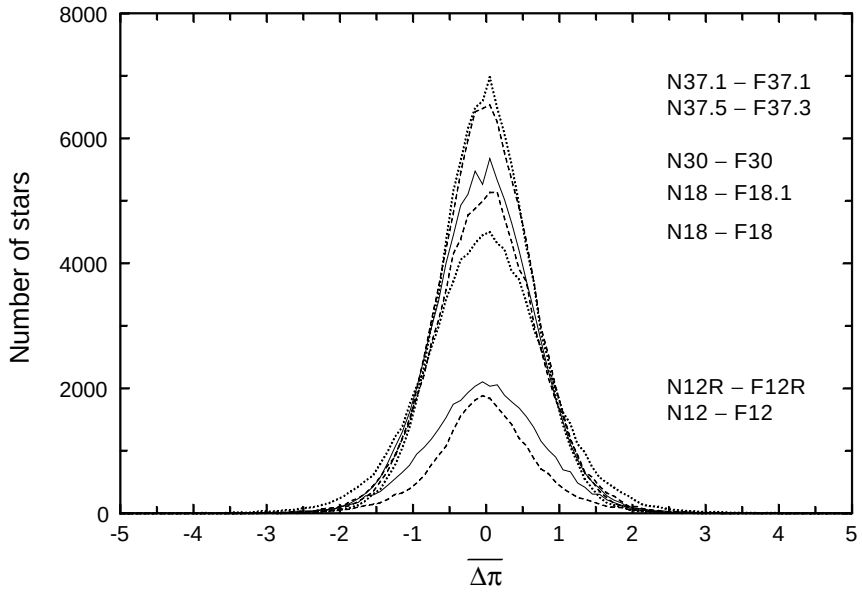

Figure 16.28. *Distributions of the normalised differences in parallax between the NDAC and FAST solutions (Equation 16.23).*

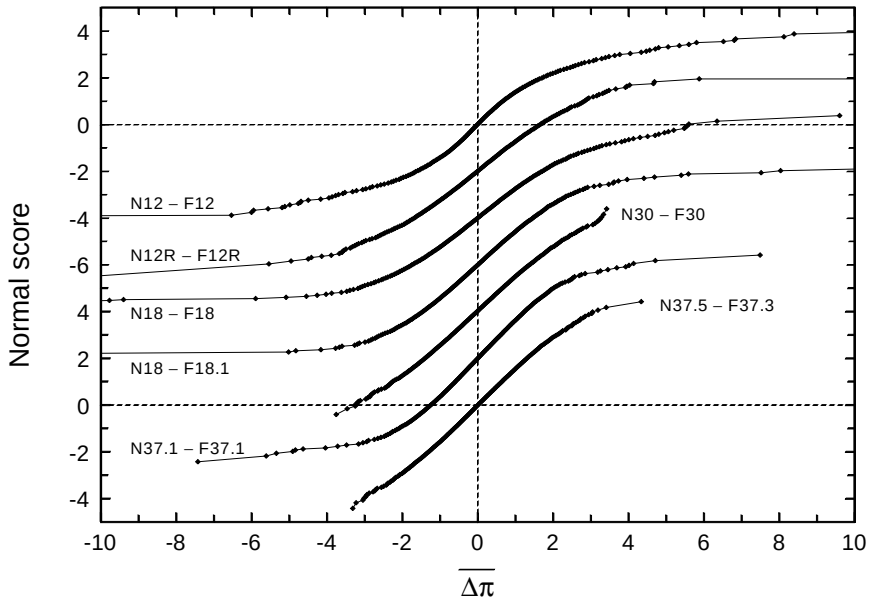

Figure 16.29. *Distributions of the normalised differences in parallax between the NDAC and FAST solutions (same as in Figure 16.28) shown as normal probability plots. A Gaussian distribution would give a straight line in this plot. The top and bottom curves are plotted against the scales shown on the left axis; other curves are vertically displaced by 2, 4, . . . units for improved visibility. The distributions of N37.5–F37.3 and N30–F30 are very nearly Gaussian, while the other distributions have more extended wings.*

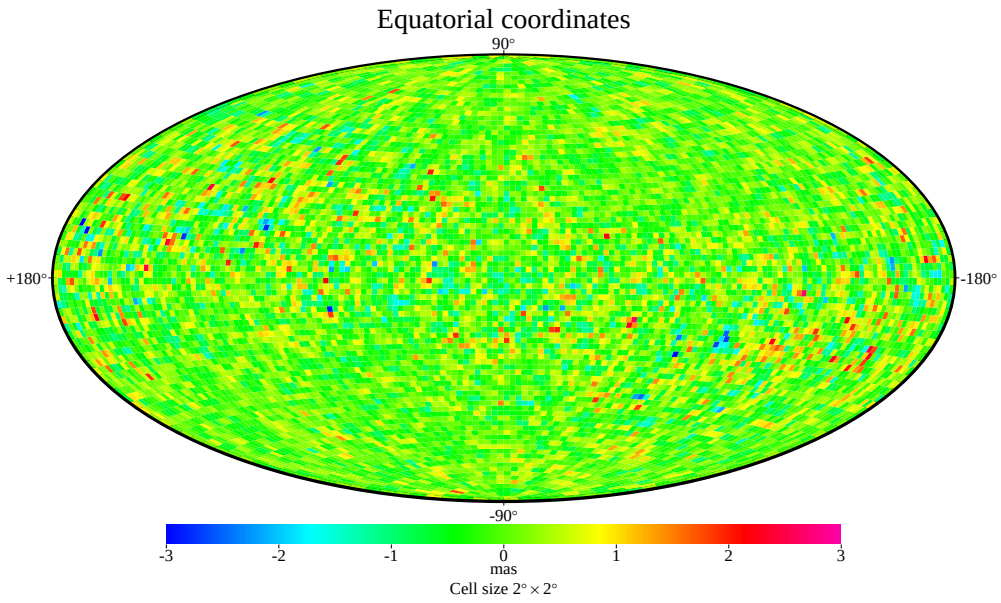

Figure 16.30. *Map of differences in right ascension between the final NDAC and FAST sphere solutions, $\Delta\alpha* = N37.5–F37.3$. Mean differences were computed in cells of $2° \times 2°$.*

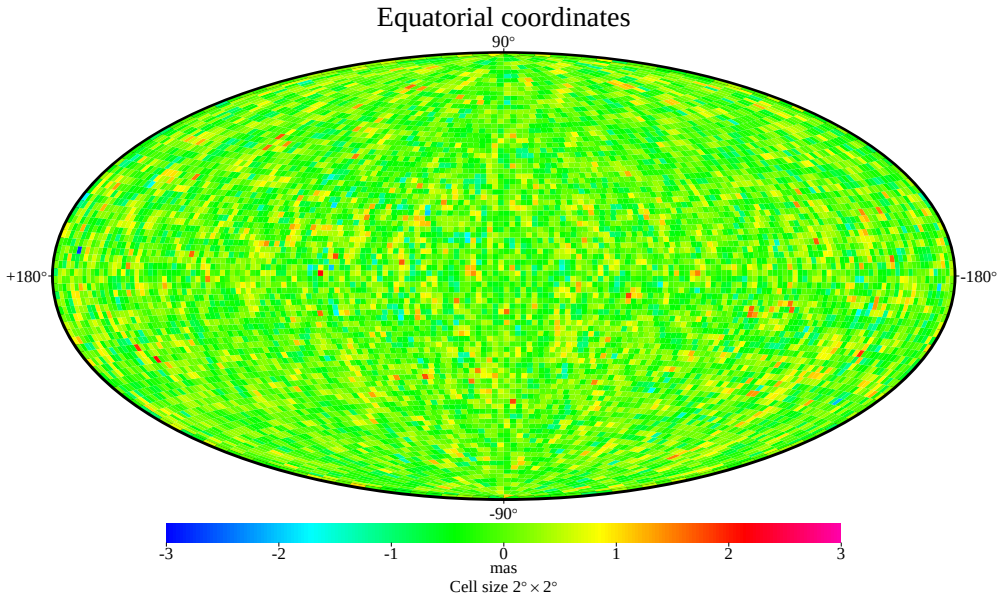

Figure 16.31. *Map of differences in declination between the final NDAC and FAST sphere solutions, $\Delta\delta = N37.5–F37.3$. Mean differences were computed in cells of $2° \times 2°$.*

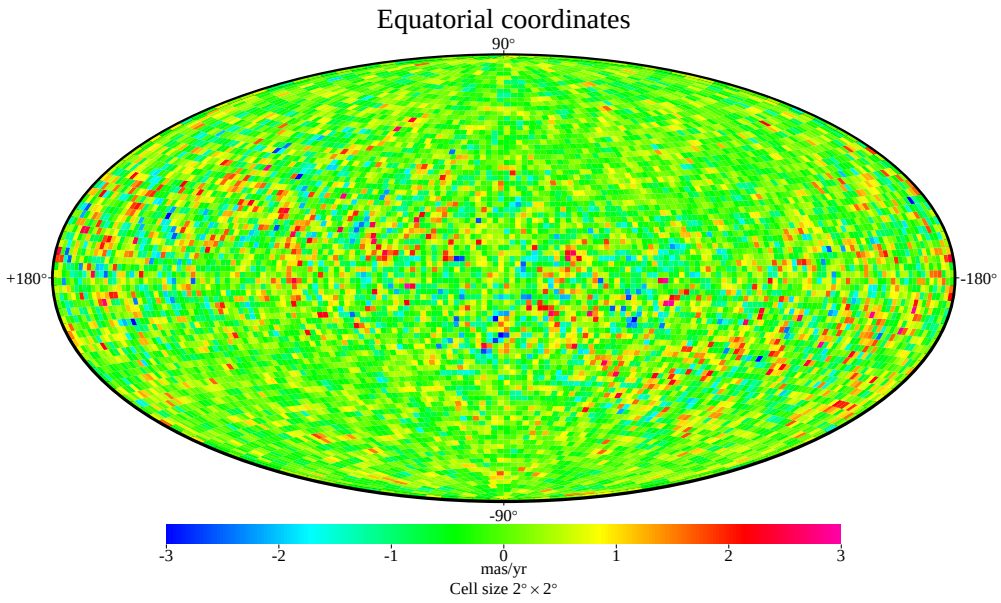

Figure 16.32. *Map of differences of proper motions in right ascension between the final NDAC and FAST sphere solutions, $\Delta\mu_{\alpha*}$ = N37.5–F37.3. Mean differences were computed in cells of $2^\circ \times 2^\circ$.*

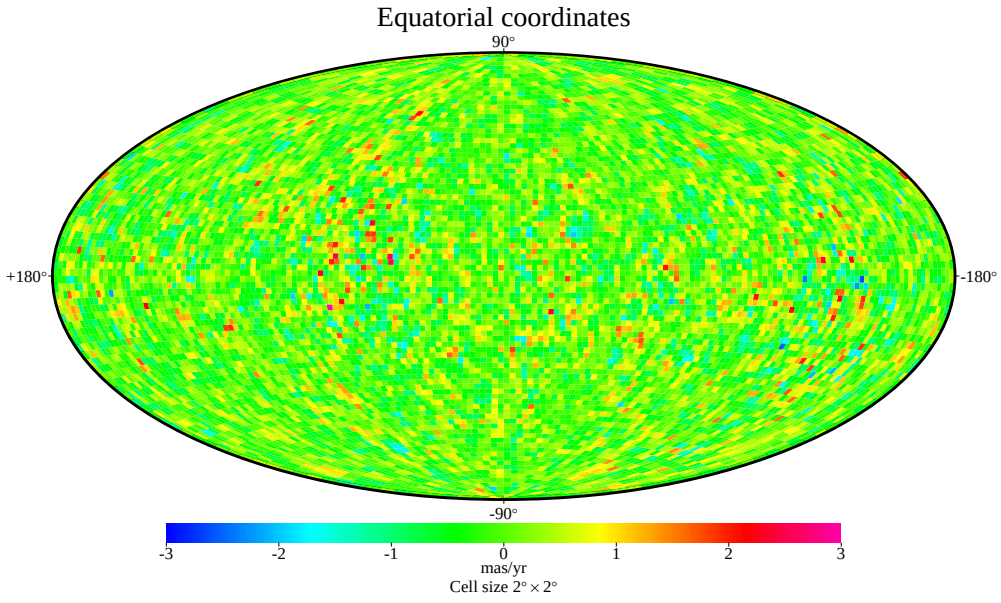

Figure 16.33. *Map of differences of proper motions in declination between the final NDAC and FAST sphere solutions, $\Delta\mu_\delta$ = N37.5–F37.3. Mean differences were computed in cells of $2^\circ \times 2^\circ$.*

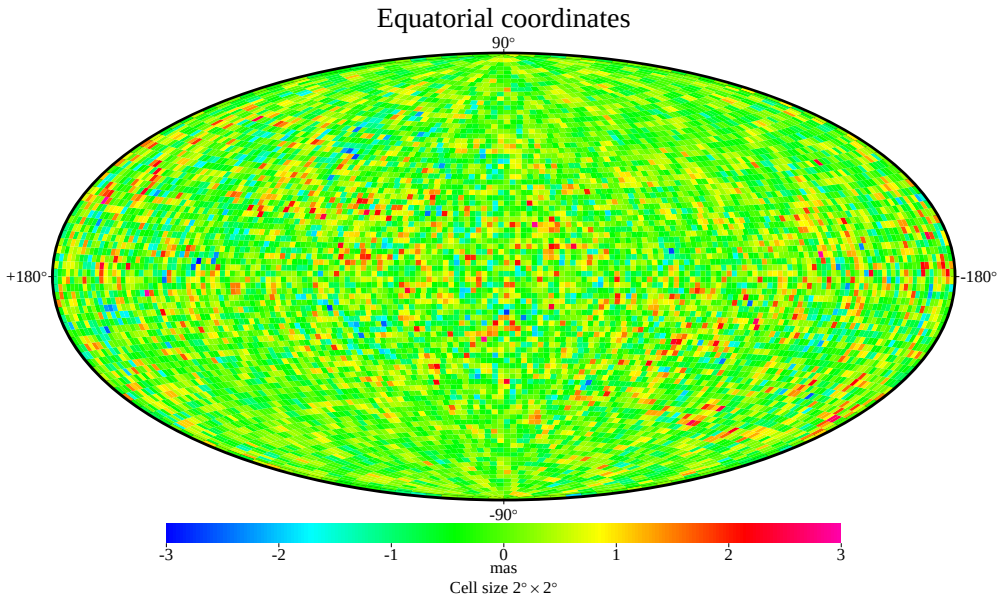

Figure 16.34. *Map of differences in parallax between the final NDAC and FAST sphere solutions, $\Delta\pi$ = N37.5–F37.3. Mean differences were computed in cells of $2^\circ \times 2^\circ$.*

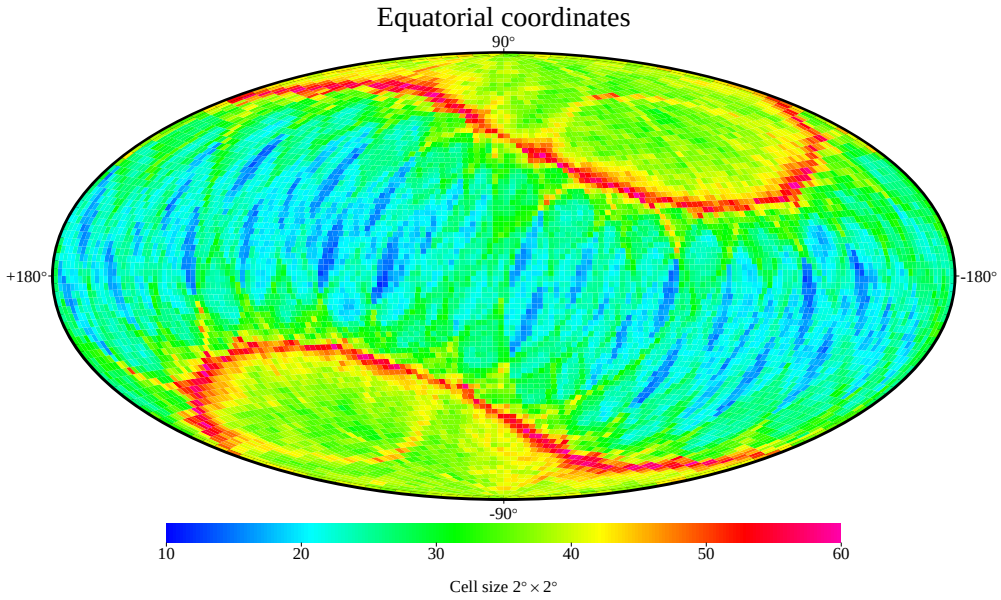

Figure 16.35. *Map of the mean number of abscissae per star used in the final solutions N37.5 and F37.3. Mean values were computed between the NDAC and FAST numbers; these were then averaged in cells of $2^\circ \times 2^\circ$.*

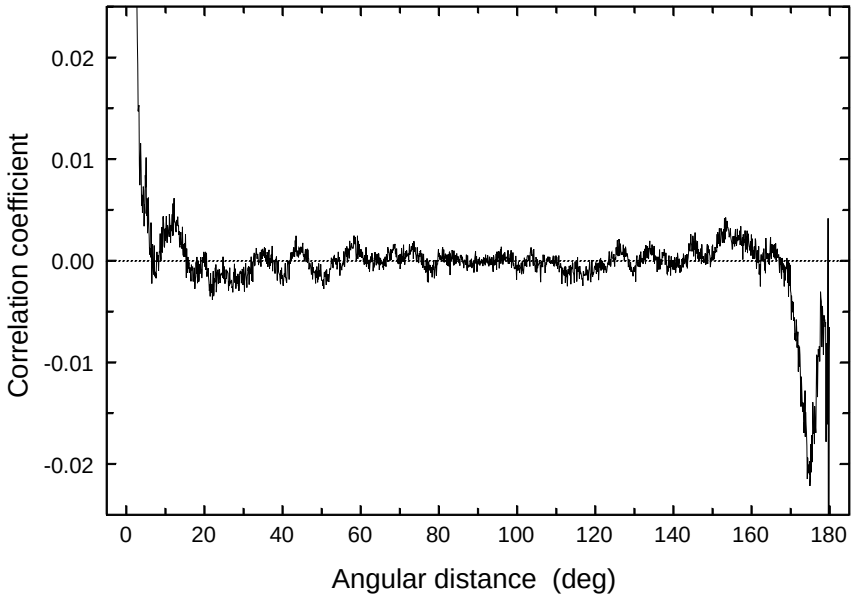

Figure 16.36. *Mean sample correlation coefficient of the normalised parallax difference ($\overline{\Delta\pi}$) as a function of angular separation. The first part of the curve is shown in more detail in the next figure.*

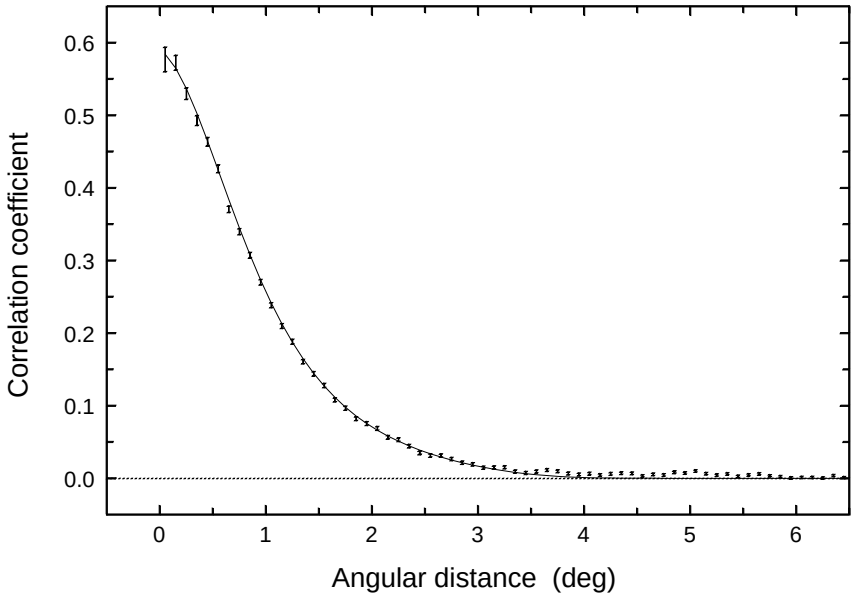

Figure 16.37. *The points with error bars give the sample correlation coefficients as in the previous figure, but only for small angular separations. The solid curve is the fitted analytical function in Equation 16.26.*

Intercomparison by the Method of Infinitely Overlapping Circles

An independent investigation into possible systematic errors remaining in the Hipparcos astrometric results after the final sphere iteration was conducted by B. Bucciarelli and M. Lattanzi, following the prescriptions of a similar study performed on the FAST and NDAC 30-month solutions (Kovalevsky *et al.* 1995). The catalogues compared were the final FAST and NDAC catalogues (F37.3 and N37.5) and the merged catalogue before rotation to the extragalactic system (H37C).

The method of infinitely overlapping circles was used; see Bucciarelli *et al.* (1994), and references therein. Briefly, the method consists of a generalised moving mean algorithm used to find an optimum weighting of the stars in order to evaluate the local systematic differences between two catalogues. For each star (the 'central star'), the catalogue differences are averaged over all stars within a certain radius R of the central star, using the weights:

$$w(r) = \frac{2}{\pi}\left[\arccos(r/R) - (r/R)\sqrt{1-(r/R)^2}\right], \quad 0 \le r \le R \qquad [16.28]$$

depending on the angular distances r of the contributing stars from the central star. The central star enters with full weight, since $w(0) = 1$. By using such a definition of statistical weight one naturally generates continuous systematic differences, while still treating the random part of the individual residuals in a statistically correct way, i.e. the formal expectation of the random part is still zero.

For the present investigation the radius of the small circle was set to $R = 2°$, giving an average of about 30 stars per circle. This choice was driven by the requirement to minimise the influence of random errors, while still probing small-scale systematics. This instance is crucial insofar as the random errors of the astrometric parameters are of the same order of magnitude, and even larger, than the systematic effects that are investigated. The method was applied to all five astrometric parameters as a function of position on the celestial sphere. As a representative example of the results, Figure 16.38 shows the average parallax differences as a function of ecliptic latitude and longitude. As expected, the values are small and, when interpreted as residual systematics of one of the two catalogues, they are typically of the order of, or less than, 0.1 mas.

Another powerful way of internally checking the statistical properties of the Hipparcos Catalogue is to compare the empirical distributions of the normalised differences between the NDAC and FAST catalogues with the theoretical distribution. In each astrometric parameter (a, e.g. ecliptic longitude) the test statistic is:

$$\epsilon_a = \frac{|a_N - (a_F + \Delta a_{NF})|}{\sqrt{\sigma_N^2 + \sigma_F^2 - 2\rho_{NF}\sigma_N\sigma_F}} \qquad [16.29]$$

where σ_N^2 and σ_F^2 are the variances of the parameter a in the two catalogues and Δa_{NF} is the catalogue-to-catalogue systematic difference (in the sense NDAC–FAST) derived with the averaging technique of the infinitely overlapping circles; ρ_{NF} is the assumed correlation between the catalogues. The predicted distribution for the test statistic ϵ_a is a folded Gaussian with a mean of $\sqrt{2/\pi} = 0.798$ and a standard deviation of $\sqrt{1-2/\pi} = 0.603$. The actual values of the first two moments of the distributions are in good agreement with the theoretical expectations.

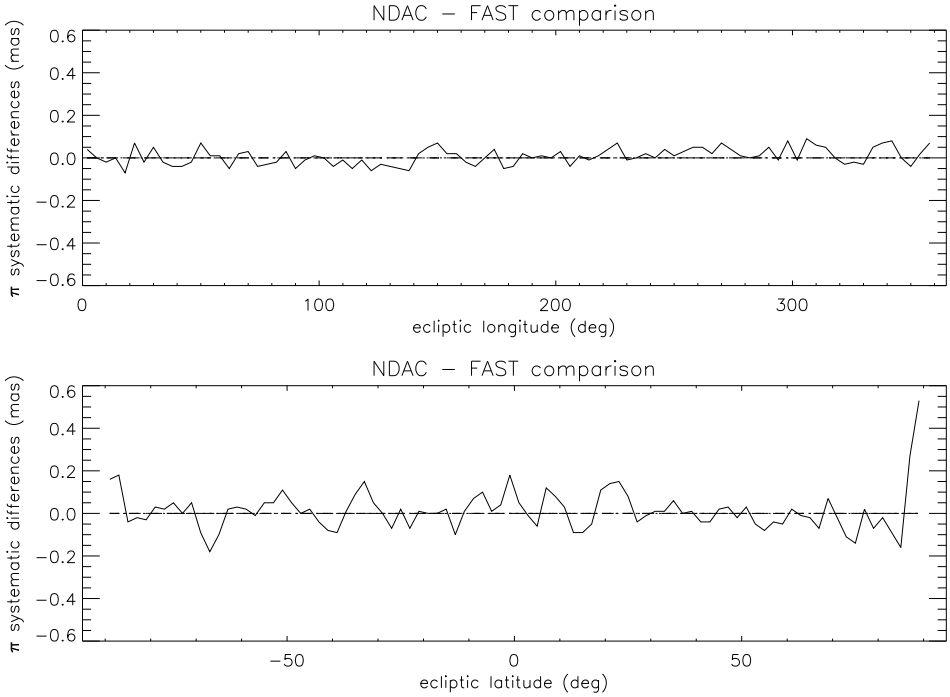

Figure 16.38. *Residual systematic differences in parallax between the final FAST and NDAC sphere solutions, plotted as a function of ecliptic longitude (top panel) and latitude (bottom panel). The data were binned in intervals of 4° and 2°, respectively.*

Note that the distribution of ϵ_a is degenerate for the case of complete overlap between the two catalogues. However, to obtain the results shown in Figure 16.39 and discussed below, a correlation coefficient $\rho_{\mathrm{NF}} = 0.79$ was assumed, i.e. some 15 per cent lower than could be expected from theoretical considerations. Part of the foundation for such a diminishment of the catalogue-wise correlation coefficient is the different processing paths adopted by the two consortia, which differentiate the catalogues more than would be expected from the number of common observations, thereby lifting (in practice) the apparent degeneracy of the problem.

Figure 16.39 shows the empirical distribution functions ϵ_λ, ϵ_β, $\epsilon_{\mu_{\lambda*}}$, ϵ_{μ_β}, and ϵ_π and their theoretical counterparts. Mean and standard deviation values of the empirical distributions are reported in Table 16.14. The bottom right diagram in Figure 16.39 was obtained by comparing the FAST catalogue with the merged one—the corresponding comparison for NDAC yields similar results. In this case the correlation coefficient which gave the best estimation of $\langle\epsilon_\pi\rangle$ and σ_{ϵ_π} (0.759 and 0.576 respectively) was $\rho_{\mathrm{FH}} = 0.96$, instead of 0.79 found for the NDAC–FAST comparison. This increase in the empirical correlation was expected as the merged catalogue is basically a weighted combination of the consortia catalogues.

In all cases a relatively small number of outliers were found ($\lesssim 3$ per cent), which were not taken into account in the calculation of the mean values. The presence of such outliers is usually explained as a discrepancy between the actual differences and the formal errors given in the catalogues.

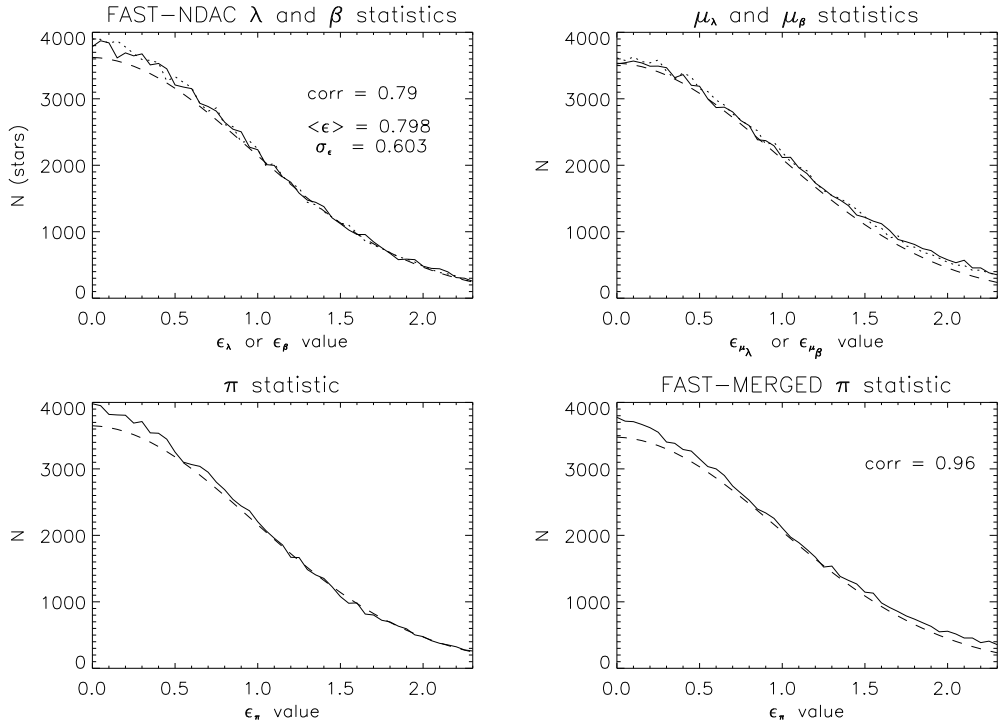

Figure 16.39. *The first three panels (from top left) show the distributions of the test statistic ϵ_a comparing the NDAC and FAST results in each of the five astrometric parameters. The fourth panel (bottom right) shows the statistic ϵ_π for the comparison between the FAST and merged catalogues. Dashed curves—theoretical distributions; solid curves—observed distribution in longitude (top) or parallax (bottom); dotted curves—observed distribution in latitude.*

In conclusion, this analysis shows that the level of (internal) residual systematics is at the level of, or smaller than, what was expected from pre-launch estimates. Also, the formal errors, as tested by the ϵ_a distributions, appear to have a high degree of consistency with statistical theory.

16.7. Conclusions

The comparison of successive sphere solutions shows very clearly the progress of the data reductions as more and more observations are included, and also the significant improvements obtained by iterating the whole reduction chain (e.g. F18.1 versus F18). The FAST/NDAC comparisons revealed important systematic differences in the early sphere solutions, which were gradually eliminated as calibrations and instrument modelling improved. For the final sphere solutions F37.3 and N37.5, all comparisons indicate that the results behave extremely well, especially in view of the known limitations of the actual mission, such as the sub-optimally sampled ecliptic region. Other tests, for instance of the parallax zero point (Chapter 20), confirm this conclusion. That Hipparcos recovered the total gravitational light deflection (proportional to $(1+\gamma)/2$) to within 0.4 per cent (NDAC) or 0.2 per cent (FAST) of the value according to General Relativity, corresponding to 0.016 mas or 0.008 mas for the mean observation at right

Table 16.14. Sample mean values and standard deviations of the test statistics computed according to Equation 16.29, assuming $\rho = 0.79$.

Statistic	Mean value $\langle\epsilon\rangle$	Standard Deviation σ_ϵ
ϵ_λ	0.769	0.565
ϵ_β	0.762	0.561
ϵ_π	0.759	0.560
$\epsilon_{\mu_{\lambda*}}$	0.808	0.588
ϵ_{μ_β}	0.798	0.581
theory	0.798	0.603

angles to the solar direction, is also an impressive testimony of its ability to perform accurate global astrometry.

It must be emphasized that the comparison of the consortia solutions cannot prove anything about the quality of the Hipparcos Catalogue. It does however provide considerable insight into the properties and possible shortcomings of the solutions, and hence of the Hipparcos Catalogue. In the end, the quality of the catalogue must be judged from the results of its many applications in astronomy and astrophysics, and from future confrontations with even more accurate measurements.

L. Lindegren, M. Frœschlé, F. Mignard